Optimal fermion-qubit mappings

Mitchell Chiew¹ and Sergii Strelchuk¹

¹DAMTP, Centre for Mathematical Sciences, University of Cambridge, Cambridge CB30WA, UK (Dated: July 12, 2022)

Simulating fermionic systems on a quantum computer requires a high-performing mapping of fermionic states to qubits. The key characteristic of an efficient mapping is its ability to translate local fermionic interactions into local qubit interactions, leading to easy-to-simulate qubit Hamiltonians. Improvements in the locality of fermion-qubit mappings have traditionally come at higher resource costs elsewhere, such as in the form of a significant number of additional qubits.

We present a new way to design fermion-qubit mappings by making use of the extra degree of freedom: the choice of numbering scheme for the fermionic modes, a feature all mappings must have. This allows us to minimse the average Pauli weight of a qubit Hamiltonian – its average number of Pauli matrices per term.

Our approach leads to a rigorous notion of optimality by viewing fermion-qubit mappings as functions of their enumeration schemes. Furthermore, finding the best enumeration scheme allows one to increase the locality of the target qubit Hamiltonian without expending any additional resources.

Minimising the average Pauli weight of a mapping is an NP-complete problem in general. We show how one solution, Mitchison and Durbin's enumeration pattern, leads to a qubit Hamiltonian for simulating the square fermionic lattice consisting of terms with an average Pauli weight 13.9% shorter than previously any previously known. Adding just two ancilla qubits, we can reduce the average Pauli weight of Hamiltonian terms by 37.9% on square lattices compared to previous methods.

Lastly, we demonstrate the potential of our techniques to polynomially reduce the average Pauli weight by exhibiting n-mode fermionic systems where optimisation yields patterns that achieve $n^{\frac{1}{4}}$ improvement in average Pauli weight over naïve enumeration schemes.

I. INTRODUCTION

Simulating physical systems is one of the most promising applications of quantum computers. Fermionic systems are essential components in several fields of theoretical and experimental physics, from quantum physics [2–5] to quantum chemistry and condensed matter [6–8] to quantum field theories [9]. Fermions pose complex, often intractable computational challenges when studied with the aid of classical computers, such as the electronic structure problem [10], studying properties of gauge theories that govern strong interactions between quarks and gluons [11], determining ground state properties of fermionic Hamiltonians [12] and many others.

One can break down all quantum algorithms for fermionic simulation into three sequential steps, depicted in Figure 1: 1) initialising the quantum register, 2) applying unitary gates to the qubits, and 3) measuring the result to obtain an estimate for the desired molecular property or other quantity of interest. Within this framework, algorithms may encode the fermionic Hamiltonian via first or second quantisation. Fermi-Dirac statistics impose asymmetry on fermionic systems' wavefunctions, and using first quantisation of the system's Hamiltonian, one can incorporate this asymmetry into the qubit basis itself or use the gubits to directly encode the wavefunction into real-time and real-space [13–16]. In contrast, second quantisation encodes the asymmetry into the qubit operators rather than the quantum states [17], and provides a number of distinct advantages over representations in the first quantisation [18, 19].

Quantum algorithms employing second quantisation require an important fourth, pre-emptive step: the fermion-qubit mapping, which we label 0) in Figure 1. In the second quantisation picture, a quantum algorithm must map each term of the fermionic Hamiltonian into a sequence of Pauli matrices acting on qubits. The original problem thus becomes a k-local Hamiltonian problem, where k depends on the choice of fermion-qubit mapping.

This work introduces a new approach to designing fermion-qubit mappings, which directly leads to a significant reduction in the complexity of some quantum simulation algorithms. There is practical value in any improvement to the sleekness of quantum simulation algorithms' designs. While the k-local Hamiltonian problem is QMA-complete [20], enormous value remains in finding or approximating solutions in the average casescenarios for practical problems, such as molecular electronic structure [21]. Turning from complexity theory, then, to focus on the more practical elimination of redundant costs in steps 0)-3) of existing fermionic simulation algorithms, there have been a number of recent developments in quantum computing that could make solutions to the above problems feasible [13–17, 21, 22]. Many of these approaches [13, 14] rely on phase estimation [23, 24] and thus require an impractically large number of qubits and operations in order to keep the register of the quantum computer coherent [?]. Algorithms for near-term quantum computers have sprung up in answer to these challenges, such as the variational quantum eigensolver [17, 25, 26], which are only just coming within reach of current technology.

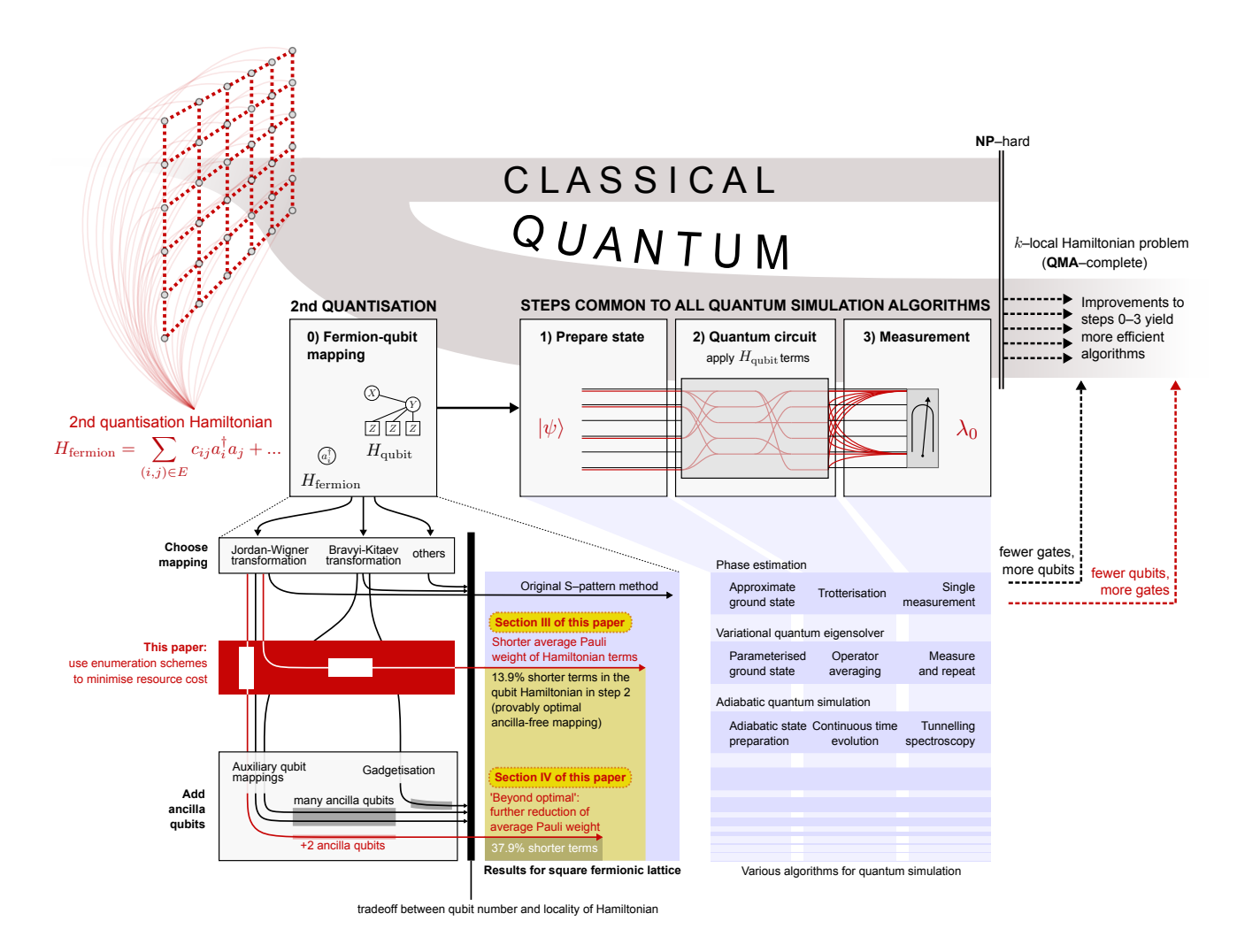


Figure 1: The general structure of a quantum simulation algorithm involves 1) preparing a quantum state, 2) running it through a quantum computer, and 3) measuring the output. Second-quantisation algorithms also require 0) a fermion-qubit mapping. One way to reduce the gate-count of a simulation algorithm is to augment its fermion-qubit mapping with ancilla qubits. In this work, we propose a more elementary improvement: optimising the fermionic enumeration scheme. Section III shows that, on the square fermionic lattice, this reduces the average Pauli weight of the qubit Hamiltonian terms by 13.9%, when compared to the previous ancilla-free method. In Section IV, we show that just two ancilla qubits can improve the reduction to 37.9%.

Mappings on the	JW [18]	This work (III)	This work (IV)	BK superfast	[27] VC [18]	AQM [28]
$N \times N$ lattice	(S-pattern)	(pattern from [1])	(+2 qubits)			
Qubit number	N^2	N^2	$N^2 + 2$	$2N^2 - 2N$	$2N^2$	$2N^2 - N$
Qubit/mode ratio	1	1	$1 + \frac{2}{N^2}$	$2 - \frac{2}{N}$	2	$2 - \frac{1}{N}$
$\operatorname{Max} XX$ hopping weight	2N	$0.2N^2 + 0.4N$	$0.12N^2 + 0.27N$	$\mathcal{O}(1)$	$\mathcal{O}(1)$	$\mathcal{O}(1)$
Average XX hopping weight	$\frac{1}{2}N + \frac{3}{2}$	0.43N + 1.78	0.31N + 1.78	$\mathcal{O}(1)$	$\mathcal{O}(1)$	$\mathcal{O}(1)$

Table I: Comparison between fermion-qubit mappings based on the dimensions of the XZZ...ZX terms when simulating an $N \times N$ square lattice. The mapping from Section III gives the minimum average Pauli weight without the assistance of ancilla qubits, and the mapping from Section IV improves this result while also maintaining a qubit/mode ratio of $1 + \mathcal{O}\left(\frac{1}{N^2}\right)$.

Some improvements to quantum simulation algorithms come with no caveats: for example, careful parallelisation of Hamiltonian terms during Trotterisation in step 2) of a phase estimation algorithm can cancel out long strings of Pauli matrices, a simple adjustment that does not come

at the expense of any additional resources [29]. However, the search for the best fermion-qubit mapping has largely not been met with much progress because the task of simulating fermionic interactions in a complexity-theoretic sense has has been extraordinarily difficult to formalise.

To bring the problem of fermionic simulation closer to meeting constraints of near-term quantum technology, it is crucially important to establish optimal protocols that strike a balance between competing resources, such as the number of qubits, local quantum operation counts, or quantum circuit depth. This is a complex challenge, as the definition of an optimal protocol may depend on the topology of the physical system to be simulated (e.g. the optimal strategy for simulating a fermionic square lattice may be different to that of a molecule), or the limitations of the quantum hardware at hand (e.g. only permitting nearest-neighbour interactions between qubits).

The idea of fermion-qubit mappings originates in the work of Jordan and Wigner almost a century ago [30]. As a mapping from qubits to fermions, Lieb et al. used the Jordan Wigner transformation to solve the XY-model Hamiltonian classically in 1961 [31]. In 2001, Ortiz employed the transformation as a fermion-qubit mapping in the first explicit proposal of a quantum simulation of a fermionic Hamiltonian [22]. The Jordan-Wigner transformation is intuitive and performs well in simulating nearest-neighbour Hamiltonians acting on 1D chains of fermionic modes, but experiences impracticably large overheads in higher dimensions.

Fermionic systems that permit only local interactions on a 2D or 3D lattice are a major focus of study [32]. These systems are difficult to simulate, even for quantum computers, because an overwhelming number of local fermionic interactions become non-local – and hence timely and costly to simulate – once mapped to the qubit picture. In recent years, there have been a flurry of results tackling this challenge introducing new fermion-qubit mappings as well as generalising the existing ones to higher dimensions [28, 33–36]. A common theme among these proposals is the use of ancilla qubits [18, 28, 35]. Such mappings can produce local qubit Hamiltonians, and could make small instances of a problem within reach of fairly modest quantum computers.

Our new approach makes use of an entirely overlooked degree of freedom of fermion-qubit mappings in higher dimensions: the ability to index the fermionic modes in any order, a process we dub *choosing the fermionic enumeration scheme*. While trivial on a 1D fermionic lattice, the choice of enumeration scheme has the potential to dramatically improve the average locality of the mapping in 2D and above. Examining enumeration schemes, and finding the most efficient ones, we show how to increase the locality of the target qubit Hamiltonian – reducing its quantum gate count – requiring no additional resources such as ancilla qubits!

Thus, we arrive at the crux of our work: for a given fermionic system and a given quantum computing technology, a fermion-qubit mapping cannot be considered optimal unless the fermionic enumeration scheme minimises the scarcest physical resource. Many innovations in fermion-qubit mappings have been in aid of reducing the maximum number of qubits upon which any one term

in the Hamiltonian acts [27, 28, 34, 35] This is an important metric in a complexity-theoretic sense – it is the 'k' in 'k–local Hamiltonian'.

We contest that other metrics may be more practical in some near-term quantum algorithms. For example, the number of Pauli measurements in a variational quantum eigensolver depends on the overall number of Pauli matrices appearing in all terms in the qubit Hamiltonian, not just the longest term. While our method could be tailored to improve many metrics of fermion-qubit mappings, the focus of this work is on improving the average locality of the qubit Hamiltonian terms. Other than a discussion on a theoretical lower bound [36], we believe this paper is the first to focus on minimising the average Pauli weight of fermion-qubit mappings.

In a fermionic Hamiltonian with non-local hopping terms, we show that minimising the average Pauli weight of a Jordan-Wigner type mapping is equivalent to the **edgesum problem** from graph theory [1, 37–39]. When compared to the only other ancilla-free mapping for the 2D fermionic lattice – which uses the S–pattern enumeration scheme, introduced by Verstraete and Cirac [18] – our method directly reduces the average Pauli weight of the terms in the qubit Hamiltonian by a constant factor ($\approx 13.9\%$). Our optimal fermion-qubit mapping uses a carefully selected enumeration scheme based on a special pattern recognised by Mitchison and Durbin in their seminal work [1], and culminates in:

Theorem 1 [Informal] For a Hamiltonian acting on a system of $n = N^2$ local fermionic modes arranged in a square $N \times N$ lattice, any fermionic enumeration scheme that follows the Mitchison-Durbin pattern also minimises the average Pauli weight of the qubit Hamiltonian.

The structure of the paper is as follows: in Section II we provide a self-contained introduction to fermion-qubit mappings and the weight of terms in the qubit Hamiltonians they produce. We follow with results from complexity theory that will be used to prove our main result.

In Section III we introduce the concept of fermionic enumeration schemes, and present Theorem 1 for constructing optimal enumeration schemes for 2D fermionic lattices in the sense that they minimise the average Pauli weight of qubit Hamiltonian terms. We argue that our approach can improve simulations for many fermionic systems, and use an heuristic approach to find enumeration schemes for certain n-mode fermionic systems that provide average Pauli weights shorter than those of naïve alternatives by a factor of $\mathcal{O}(n^{1/4})$.

In Section IV, we explain the auxiliary qubit mapping technique and modify our fermion-qubit mapping to improve Theorem 1's 13.9% advantage over the S-pattern to nearly 38% using just two ancilla qubits.

Finally, in Section V we argue that our approach can adjust to reduce other figures of merit such as circuit depth, or to cluster the Hamiltonian terms closer together on specific qubit architectures, which could improve qubit routing protocols.

II. BACKGROUND

This section provides the necessary background for the Jordan-Wigner transformation on fermionic systems (Sections II A–II D), and details relevant graph problems and complexity theory (Section II E).

A. Canonical anticommutation relations

In order to describe the possible interactions in a system of n fermionic modes, it is necessary to label each mode with an integer from 1 to n. This is the first step of any fermion-qubit mapping, and here we call it the process of choosing a fermionic enumeration scheme. The fermionic system has a state space, known as Fock space, with the occupancy number basis $\{|j_1, j_2, \ldots, j_n\rangle \mid j_i \in \{0, 1\}\}$ where j_i denotes the occupancy of the ith fermionic mode. We use the term fermionic mode as in [27], where a mode can either be empty or occupied. The annihilation operators a_i act on the Fock space as

$$a_i|j_1...\underbrace{0}_{i\text{th place}}...j_n\rangle = 0$$
 (1)

$$a_i|j_1...\underbrace{1}_{i\text{th place}}...j_n\rangle = (-1)^{\sum_{k=1}^{i-1}j_k}|j_1...\underbrace{0}_{i\text{th place}}...j_n\rangle,$$
 (2)

while their Hermitian conjugates, the creation operators, act on the system as a_i^{\dagger} . Equations 1 and 2 are equivalent to Equations 3, 4 and 5 [40], which are the *canonical anticommutation relations*:

$$\{a_i, a_k\} = 0 \tag{3}$$

$$\{a_i^{\dagger}, a_k^{\dagger}\} = 0 \tag{4}$$

$$\{a_i, a_k^{\dagger}\} = \delta_{ik} \mathbb{1}. \tag{5}$$

B. Fermion-qubit mappings

Consider a general Hamiltonian H which encodes the dynamics of a fermionic system with n modes,

$$H_{\text{fermion}} = \sum_{\alpha} c_{\alpha} O_{\alpha} , \qquad (6)$$

where each O_{α} is the product of an equal number of creation and annihilation operators, ensuring the Hamiltonian is a physical operator, and the complex coefficients c_{α} are such as to ensure that H_{fermion} is Hermitian. Suppose that we have $m \geq n$ qubits at our disposal to simulate the n-mode system. The state of a qubit system can be written in terms of the basis $\{|l_1, l_2, \ldots, l_m\rangle \mid l_i \in \{0, 1\}\}$, where l_i denotes the value of the binary observable (say, z-component of spin) of the ith qubit. Developing a fermion-qubit mapping is tantamount to finding operators \mathbb{A}_i such that $\{\mathbb{A}_i^{\dagger}, \mathbb{A}_j\} = \delta_{ij}\mathbb{I}$ and $\{\mathbb{A}_i^{(\dagger)}, \mathbb{A}_j^{(\dagger)}\} = 0$, for $i, j \in \{1, 2, \ldots, n\}$.

Property System	Basis states	Operations	
		Ladder operators a_i, a_i^{\dagger}	
n fermionic	$ j_1,j_2,\ldots,j_n\rangle$	with $\{a_i, a_j^{\dagger}\} = \delta_{ij} \mathbb{1}$,	
modes	$j_i = \text{occupancy}$	$\{a_i^{(\dagger)}, a_j^{(\dagger)}\} = 0;$	
		Physical $\propto a_i^{\dagger} a_j + a_j^{\dagger} a_i$	
$m \ge n$ qubits		Operations A_i, A_j^{\dagger} ,	
	$ l_1, l_2, \ldots, l_m\rangle$	$1 \le i \le n$, with	
	$l_i = \text{spin}$	$\{\mathbb{A}_i, \mathbb{A}_j^{\dagger}\} = \delta_{ij}\mathbb{1},$	
		$\{\mathbf{A}_i^{(\dagger)}, \mathbf{A}_j^{(\dagger)}\} = 0$	

Table II: **Top:** Basic building blocks of a fermionic system. **Bottom:** The equivalent properties of a qubit system under a fermion-qubit mapping.

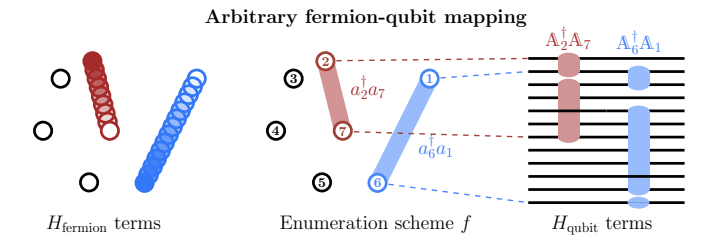


Figure 2: A fermion-qubit mapping distinguishes fermionic modes via an enumeration scheme. Via the transformations $a_i \mapsto \mathbb{A}_i$, the fermion-qubit mapping replicates the algebra of the canonical anticommutation relations on a system of $m \geq n$ qubits. This diagram depicts the qubits that the hopping terms act on, and should not be interpreted as a quantum circuit.

Table II summarises the analogues between fermion and qubit systems and Figure 2 illustrates a very general picture of an arbitrary fermion-qubit mapping. All known fermion-qubit mappings in the literature are a subset of the template described in these two figures.

The most widely-used fermion-qubit mappings, the Jordan-Wigner [30] and Bravyi-Kitaev [27] transformations, simulate Hamiltonians on n fermionic modes with n qubits. A considerable repertoire of fermion-qubit mappings has developed in recent years, each with its own strengths and weaknesses. Mappings that use m>n qubits, e.g. [28, 35] transform Hamiltonian terms into chains of Pauli spin operators $(\sigma^x, \sigma^y, \sigma^z)$ and reduce the lengths of these chains with stabilisers involving auxiliary qubits. We discuss this process in Section IV, and give a novel example that simulates the fermionic lattice with m=n+2 qubits.

C. The Jordan-Wigner transformation

The Jordan-Wigner transformation is a fermion-qubit mapping that uses m = n qubits and arises naturally by

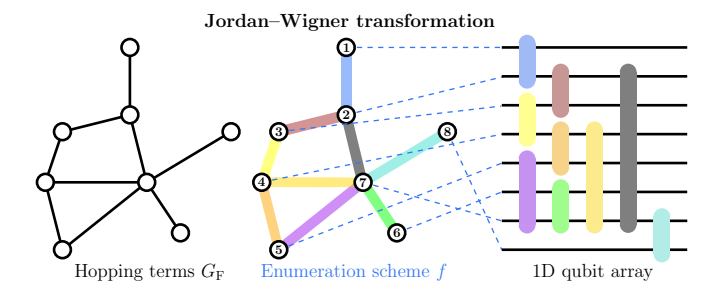


Figure 3: The Jordan-Wigner transformation converts an n-mode fermionic Hamiltonian into strings of Pauli operations on n qubits. Here, the graph $G_{\rm F}$ represents all single-particle interactions between modes in the Hamiltonian.

constructing

$$\sigma^{+} := \frac{1}{2}(\sigma^{x} - i\sigma^{y}) = \frac{1}{2}(X - Y) = |1\rangle\langle 0| \tag{7}$$

$$\sigma^{-} \coloneqq \frac{1}{2}(\sigma^{x} + i\sigma^{y}) = \frac{1}{2}(X + Y) = |0\rangle\langle 1| , \qquad (8)$$

which behave somewhat like creation-annihilation operators. Here, we use the convention $X = \sigma^x$ and $Y = i\sigma^y$. While $\{\sigma^+, \sigma^-\} = \mathbb{1}$, across multiple qubits when $i \neq j$ we have $\{\sigma_i^+, \sigma_j^-\} = |01\rangle\langle 10|_{i,j} \neq 0$, where the subscript i denotes action on the ith qubit. Thus, σ_i^- and σ_j^+ alone cannot replicate the anticommutation relations of the operators a_i and a_i^{\dagger} .

The Jordan-Wigner transformation defines the Pauli equivalents of creation and annihilation operators, A_i and A_j^{\dagger} , via

$$a_i \longmapsto \mathbb{A}_i = \left(\bigotimes_{k=1}^{i-1} \sigma_k^z\right) \sigma_i^-$$
 (9)

$$a_j^{\dagger} \longmapsto \mathbb{A}_j^{\dagger} = \left(\bigotimes_{k=1}^{i-1} \sigma_k^z\right) \sigma_j^+.$$
 (10)

Using the anticommutation relations $\{\sigma_i^{\pm}, \sigma_i^z\} = 0$, these operators preserve the fermionic algebra, as

$$\{\mathbf{A}_i, \mathbf{A}_j^{\dagger}\} = \{\sigma_i^-, \sigma_i^z\} \left(\bigotimes_{k=i+1}^{j-1} \sigma_k^z\right) \sigma_j^+ = 0 \tag{11}$$

where j > i, as is required of a fermion-qubit mapping. In our work we confine our discussion to Jordan-Wigner type mappings, which exhibit a direct and intuitive correlation between fermions and qubits. The correlation is thus: \mathbb{A}_i and \mathbb{A}_j^{\dagger} naturally act on the spin basis $\{|l_1, l_2, \ldots, l_n\rangle \mid l_i \in \{0, 1\}\}$ in exactly the same way that the fermionic creation and annihilation operators a_i and a_j^{\dagger} act on the Fock basis $\{|j_1, j_2, \ldots, j_n\rangle \mid j_i \in \{0, 1\}\}$. That is, $l_i = j_i$. This is in contrast to other fermion-qubit mappings – for example in the case of the Bravyi-Kitaev transformation [27], the operators \mathbb{A}_i and \mathbb{A}_j^{\dagger} act

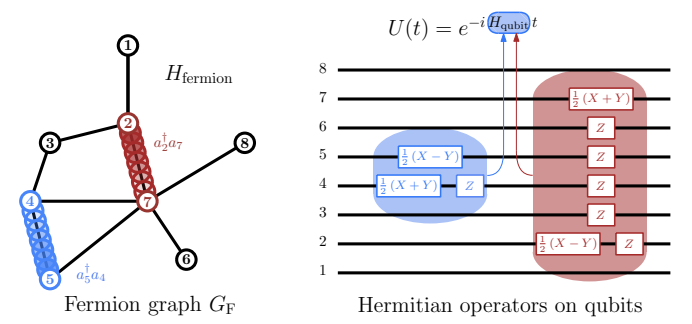


Figure 4: Visualisation of Equation 17. **Left:** representation of individual terms $a_2^{\dagger}a_7$ and $a_5^{\dagger}a_4$ in a fermionic Hamiltonian describing a system of fermions. **Right:** Jordan-Wigner transform of these terms into strings of Pauli operators acting on qubits.

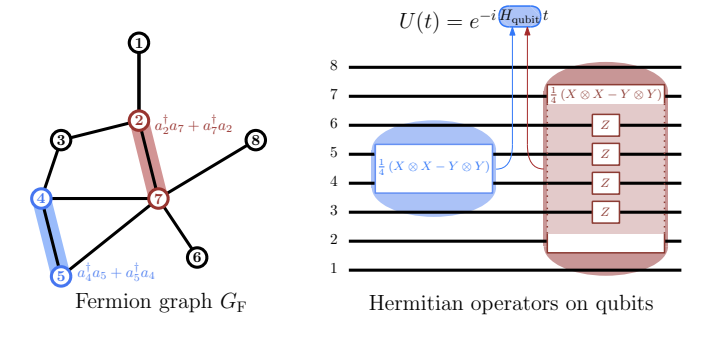


Figure 5: Visualisation of Equation 16. **Left:** as the Hamiltonian is Hermitian, every individual term of the form $a_i^{\dagger}a_j$ can pair with its Hermitian conjugate $a_j^{\dagger}a_i$. **Right:** Jordan-Wigner transform of the grouped terms $a_i^{\dagger}a_j + a_j^{\dagger}a_i$ into strings of Pauli operators acting on qubits.

on a basis for qubit space $\{|b_1, b_2, \dots, b_n\rangle \mid b_i \in \{0, 1\}\}$, with $b_i = \sum_k [B]_{ik} j_k$ where B is a specific invertible matrix. We discuss some of the merits and drawbacks of the Bravyi-Kitaev transformation in Section V B.

D. Jordan-Wigner transformation of local fermionic Hamiltonians

Typical Hamiltonians of interest, such as molecular electronic Hamiltonians, have the form

$$H_{\text{fermion}} = \sum_{\alpha\beta} (c_{\alpha\beta}) a_{\alpha}^{\dagger} a_{\beta} + \frac{1}{2} \sum_{\alpha\beta\gamma\delta} (c_{\alpha\beta\gamma\delta}) a_{\alpha}^{\dagger} a_{\beta}^{\dagger} a_{\gamma} a_{\delta} ,$$
(12)

where the indices $\alpha, \beta, \gamma, \delta$ are unordered labels for the n fermionic modes. For example, in the Fermi-Hubbard model the fermions are electrons, the coefficients $c_{\alpha\beta}$ and $c_{\alpha\beta\gamma\delta}$ are respectively one- and two-electron overlap integrals, and the summation indices run through all possible fermionic modes, including multiple excitation states of each individual electron. A Hamiltonian consisting just

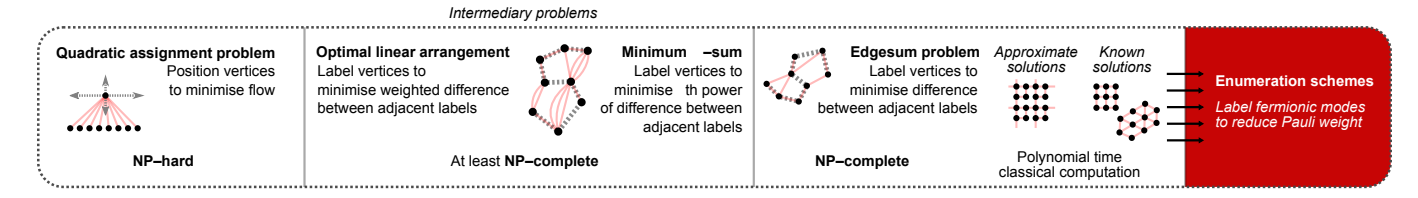


Figure 6: Complexity-theoretic hierarchy of problems generalising the edgesum problem.

of quadratic single-particle terms $a_{\alpha}^{\dagger}a_{\beta}$ may easily be diagonalised and its eigenvalues simply read off [40]. The presence of quartic terms usually makes simulation of the Hamiltonian classically intractable, and as such an object of interest for prospective quantum algorithms.

As a physical Hamiltonian, each term in Equation 12 preserves the particle number of the system. The Jordan-Wigner transformation uses a fermionic enumeration scheme f to convert the indices $\alpha, \beta, \gamma, \delta$ into numerical indices $i, j, k, l \in \{1, 2, \ldots, n\}$. It then transforms the quadratic single-fermion Hamiltonian terms, known as hopping terms, into combinations of Pauli matrices:

$$a_i^{\dagger} a_i \longmapsto \frac{1}{2} \left(\mathbb{1}_i - \sigma_i^z \right) = \frac{1}{2} \left(\mathbb{1}_i - Z_i \right)$$
 (13)

$$a_i^{\dagger} a_j \longmapsto \frac{1}{2} \left(X_i - Y_i \right) \left(\bigotimes_{k=i}^{j-1} Z_k \right) \frac{1}{2} \left(X_j + Y_j \right) , \quad (14)$$

where i < j in Equation 14, and $Z = \sigma^z$.

Literature on quantum simulation algorithms tends to permit quartic terms in the fermionic Hamiltonian that transform into local qubit operations. For example, Verstraete and Cirac [18] and Derby and Klassen [35] consider terms of the form

$$a_i^{\dagger} a_i a_j^{\dagger} a_j \longmapsto \frac{1}{4} (\mathbb{1}_i - Z_i) (\mathbb{1}_j - Z_j).$$
 (15)

These quartic terms make diagonalisation of the

fermionic Hamiltonian H difficult, but they become simple 1- or 2-local Pauli operations after the Jordan-Wigner transformation maps them into qubit Hamiltonian terms. Thus, the main contributor to the cost of simulating the qubit Hamiltonian is the length of the hopping terms of the form in Equation 14.

Figure 3 visualises how the Jordan-Wigner transformation maps the hopping terms in a fermionic system into Pauli strings. Here we use the graph $G_{\rm F}$ to describe the hopping terms, where the fermionic Hamiltonian only includes hopping term $a^{\dagger}_{\alpha}a_{\beta}$ if (α,β) is an edge of $G_{\rm F}$.

After using an enumeration scheme for the fermions, Figure 4 demonstrates the transformation of hopping terms $a_2^{\dagger}a_7$ and $a_5^{\dagger}a_4$. However, the term $c_{ij}a_i^{\dagger}a_j$ will always appear in H alongside its conjugate term $(c_{ij})^*a_j^{\dagger}a_i$. Thus the qubit Hamiltonian will exhibit non-local terms of the form in Equation 17.

In the case when the coefficients of the grouped terms are $c_{ij} = (c_{ij})^* = 1$, the transformation is simply

$$a_i^{\dagger} a_j + a_j^{\dagger} a_i \longmapsto \frac{1}{2} \left(\bigotimes_{k=i+1}^{j-1} Z_k \right) \left(X_i \otimes X_j - Y_i \otimes Y_j \right).$$
 (16)

Figure 5 illustrates the conversion of conjugate hopping terms of the form of Equation 16 into quantum circuits.

$$c_{ij}a_i^{\dagger}a_j + (c_{ij})^*a_j^{\dagger}a_i \longmapsto \frac{\operatorname{Re}(c_{ij})}{2} \left(\bigotimes_{k=i+1}^{j-1} Z_k\right) (X_i \otimes X_j - Y_i \otimes Y_j) + \frac{i\operatorname{Im}(c_{ij})}{2} \left(\bigotimes_{k=i+1}^{j-1} Z_k\right) (Y_i \otimes X_j - X_i \otimes Y_j). \tag{17}$$

The remainder of this paper will detail new ways to reduce the average number of matrices in these non-local qubit operations on a case-by-case basis, by careful choice of the fermionic enumeration scheme.

E. Complexity-theoretical preliminaries

This section introduces the necessary notation and complexity theoretic problems that underpin our results.

A visual summary of the hierarchy of these problems appears in Figure 6. All problems start with some variation of the following ingredients:

- 1. A graph G = (V, E) with |V| = n vertices and edge set $E \subseteq V \times V$, and
- 2. a weight function $w: E \to \mathbb{R}$, which assigns a value $w(\alpha, \beta)$ to the edge (α, β) between vertices $\alpha, \beta \in V$, and
- 3. a list L of possible **locations** for the vertices, and

4. a distance function $d: L \times L \to \mathbb{R}$ describing the spatial separation between the locations.

This section lists graph problems relevant to the discussion in this paper. All problems have the objective of finding an injective **assignment function** $f:V\to L$ to place the vertices in locations so as to minimise a cost function. We call f an *enumeration scheme* when $L=\{1,2,\ldots,n\}$,

1. NP-hard problems

The following problem was shown by Koopmans [41] to be NP-hard:

QUADRATIC ASSIGNMENT

INSTANCE: Graph G = (V, E), weight function $w : E \to \mathbb{R}$, vertex locations L, distance function $d : L \times L \to \mathbb{R}$.

PROBLEM: Find the location assignment function $f: V \to L$ in such a way as to minimise the cost function

$$C(f) = \sum_{(\alpha,\beta)\in E} w(\alpha,\beta) \cdot d(f(\alpha), f(\beta)) . \quad (18)$$

2. Problems that are at least NP-complete.

The following problems appear to generalise some NP-complete problems, however it is unknown if they are NP-complete themselves or if they are actually NP-hard.

The optimal linear arrangement problem was first studied by Garey and Johnson [37]. Note that it is different to the "optimal linear arrangement" in their book [39].

OPTIMAL LINEAR ARRANGEMENT

INSTANCE: Graph G = (V, E), weight function $w : E \to \mathbb{Z}$.

PROBLEM: Find the enumeration scheme $f: V \to \{1, 2, \dots, n\}$ that minimises cost function

$$C(f) = \sum_{(\alpha,\beta)\in E} w(\alpha,\beta) \cdot |f(\alpha) - f(\beta)| . \quad (19)$$

This is a special case of the quadratic assignment problem: the weight function w is restricted to integer values, the vertex locations L are $\{1,2,\ldots,n\}$, and the distance metric is d(i,j)=|i-j|. According to Horton [42], it is not known whether the optimal linear arrangement problem as written here is NP-hard or NP-complete.

The minimum p-sum problem was studied by Mitchison and Durbin [1], Garey and Johnson [38], and Juvan and Mohar [43].

MINIMUM p-SUM

INSTANCE: Graph G = (V, E), integer $p \in \mathbb{Z}$. **PROBLEM**: Find the enumeration scheme $f: V \to \{1, 2, \dots, n\}$ that minimises cost function

$$C^{p}(f) = \left(\sum_{(\alpha,\beta)\in E} |f(\alpha) - f(\beta)|^{p}\right)^{1/p}.$$
 (20)

This is a special case of the optimal linear arrangement problem, because its weight function is effectively $w(\alpha,\beta) = |f(\alpha) - f(\beta)|^{p-1} \in \mathbb{Z}$. This problem is NP-complete for p=1 [37], p=2 [44] and $p\to\infty$ [42]. One could also consider the broader class of problems where $p\in\mathbb{R}^+$, as done by Mitchison and Durbin [1]. These problems are likely to be at least as hard as their integer-p equivalents.

3. NP-complete problems.

The edgesum problem was introduced in [37], and the study of this problem is the key ingredient to our optimal fermion-qubit mappings:

EDGESUM (or SIMPLE OPTIMAL LINEAR ARRANGEMENT, MINIMUM 1-SUM)

INSTANCE: Graph G = (V, E).

PROBLEM: Find the enumeration scheme $f: V \to \{1, 2, \dots, n\}$ that minimises cost function

$$C(f) = \sum_{(\alpha,\beta)\in E} |f(\alpha) - f(\beta)|.$$
 (21)

Figure 7 surveys the graphs with known solutions, as of the date of publication of Hortons's PhD thesis [42] which cites a solution for outerplanar graphs by Frederickson and Hambrusch [46]. Other sources include a survey by Lai [45], and solution for tree graphs by Chung [47]. This problem is known to be NP-complete via a reduction to the simple max-cut problem [37].

As an example of a comparable problem, consider the following:

BANDWIDTH (or MINIMUM ∞-SUM)

INSTANCE: Graph G = (V, E).

PROBLEM: Find the enumeration scheme $f: V \to \{1, 2, \dots, n\}$ that minimises cost function

$$\max_{(\alpha,\beta)\in E} |f(\alpha) - f(\beta)| . \tag{22}$$

This is the minimum p-sum problem as $p \to \infty$. The bandwidth problem is NP-complete for an arbitrary tree

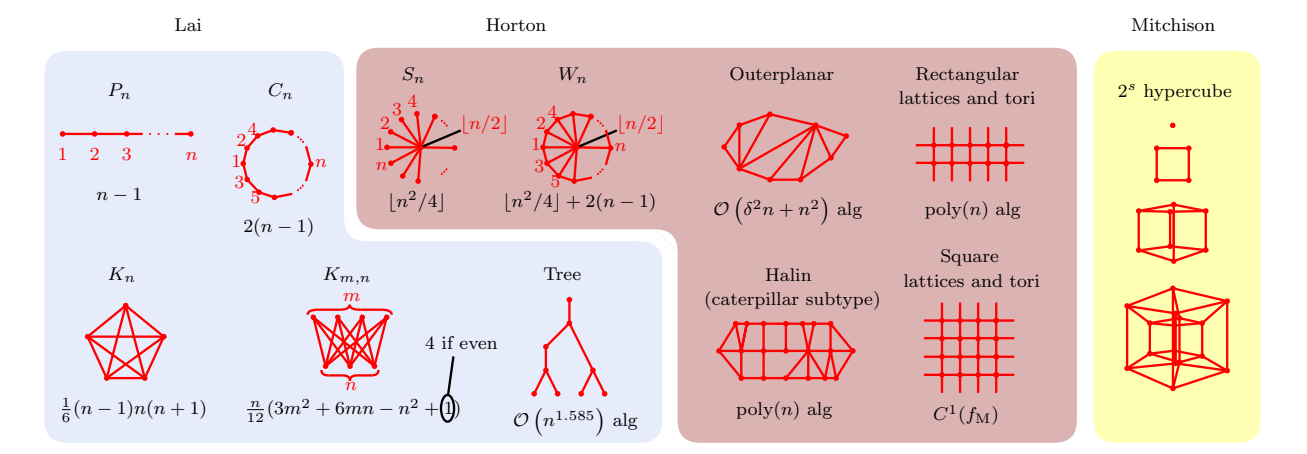


Figure 7: Graph families with known solutions to their edgesum problems. The formula for the minimum edgesum appears beneath each graph's image, if it exists, or the cost of the best-known classical algorithm for solving that graph's edgesum problem if not. References for the solution of these graphs appear in Lai [45], Horton [42], and Mitchison's [1] works as indicated.

graph [38]. Conversely, Saxe proves that the decision problem as to whether the bandwidth is less than or equal to k = O(1) is efficiently solvable [48].

III. FERMIONIC ENUMERATION SCHEMES AND QUANTUM RESOURCES

This section introduces the key idea: using enumeration schemes to optimise fermion-qubit mappings. Section III A describes the various quantities that enumeration schemes can reduce, including the average Pauli weight. Section III B states Theorem 1 for minimising the average Pauli weight of a qubit Hamiltonian when the nonlocal terms are between vertices on a square lattice. Section III C details the proof of Theorem 1. In Section III D, we consider an heuristic approach to reducing the average Pauli weight of cellular lattice fermionic systems, by providing bespoke enumeration schemes that are better than naïve approaches. In Section III E, we consider the task of minimising the average pth power of Pauli weight in quantum circuits for simulating square lattice fermionic systems, for p > 1.

In this section, we only consider Jordan-Wigner transformations from n-mode fermionic systems to linear (1D) n-qubit systems. One might note that prior works such as the Verstraete-Cirac [18] and Steudtner-Wehner mappings [28] improve the Jordan-Wigner transformation at the seemingly low cost of using $\mathcal{O}(n)$ extra qubits, and also map onto constrained 2D lattice qubit systems. Section IV will elaborate on how the ideas for optimal Jordan-Wigner transformations presented in this section can improve with the addition of auxiliary qubits, and can adapt to fit any qubit geometry.

A. Enumeration schemes and figures of merit

Given a Hamiltonian for an n-mode fermionic system of the form in Equation 12, the first step of any Jordan-Wigner process is always to label the fermionic modes with an enumeration scheme f. The hopping term $a_{\alpha}^{\dagger}a_{\beta}$ between modes α and β is then $a_{f(\alpha)}^{\dagger}a_{f(\beta)}=a_{i}^{\dagger}a_{j}$. The Jordan-Wigner transform maps $a_{i}^{\dagger}a_{j}$ to a Pauli string on the 1D qubit array via Equation 14. As mentioned in Section II D, we only concern ourselves with the hopping terms $a_{\alpha}^{\dagger}a_{\beta}$, as they become non-local in the qubit Hamiltonian; we assume the quartic terms will become local Pauli operators. Any given enumeration scheme f thus generates a unique list of Pauli strings, corresponding to the qubit Hamiltonian's hopping terms. Figure 8 gives three examples for three different enumeration schemes.

We propose the strategy of choosing a fermionic enumeration scheme that minimises a property of its induced list of Pauli strings. This property should pertain to the efficiency of the quantum computer, be it depth, gate count, or some other measure. We define several such properties below.

1. Average Pauli weight. A Pauli operator's weight is the number of qubits it acts on. A natural property to try and minimise when choosing an enumeration scheme f is the average weight of all the Pauli strings that the Jordan-Wigner transform produces when applied to the hopping terms of the Hamiltonian. This corresponds to minimising the objective function

$$C^{1}(f) := \sum_{(\alpha,\beta) \in G_{F}} |f(\alpha) - f(\beta)|.$$
 (23)

If the connectivity graph $G_{\rm F}$ describes the hopping terms of the fermionic Hamiltonian, the formula for the average Pauli weight of enumeration scheme f

(denoted as APV(f)) is

$$APV(f) := \frac{C^1(f)}{|G_F|} + 1,$$
 (24)

where $|G_{\rm F}|$, the number of edges in $G_{\rm F}$, is also the number of hopping terms in the Hamiltonian. The extra term of 1 accounts for the fact that the weight of a Pauli string between qubits with labels i and j is |i-j|+1. Figure 8 shows the average Pauli weight on the 6×6 lattice for three enumeration schemes: the S-pattern $f_{\rm S}$, the Z-pattern $f_{\rm Z}$, and the Mitchison-Durbin pattern, $f_{\rm M}$.

The search for such an enumeration scheme is an example of the NP-complete edgesum problem from Section II E. In Section III B, we present Theorem 1 for an enumeration scheme $f_{\rm M}$ that minimises the average Pauli weight of a Jordan-Wigner mapping if $G_{\rm F}$ is a square lattice. Through Corollary 1.1, this lends an improvement to existing protocols for fermionic square lattice simulation by reducing the average Pauli weight by up to $\approx 13.9\%$.

2. Average pth power of Pauli weight. One might want to penalise the length of hopping terms via some other measure, such as the average pth power of the Pauli weights where $p \in \mathbb{R}^+$. Minimising this property corresponds to the minimum-p-sum problem from Section II E of finding the enumeration scheme f that minimises

$$C^{p}(f) := \left(\sum_{(\alpha,\beta) \in G_{\mathcal{F}}} |f(\alpha) - f(\beta)|^{p}\right)^{1/p}.$$
 (25)

In Section IIIE, we present numerical results for the minimum p-sum problem to illustrate how one might choose fermionic enumeration schemes to optimise over this objective function.

3. Other properties. One may also consider other properties. For example, if the qubits have a connectivity graph $G_{\mathbf{Q}}$, it may be desirable to make the Pauli strings as local as possible on $G_{\mathbf{Q}}$. We include a discussion of this optimisation in Section V C.

B. Minimising the average Pauli weight for a square fermionic lattice

We will now exhibit an optimal fermion-qubit mapping – one that minimises the average Pauli weight of the Jordan-Wigner-transformed qubit Hamiltonian. It turns out that the most efficient way to label fermionic modes is related to the work of Graeme Mitchison and Richard Durbin when they studied the organisation of nerve cells in the brain cortex [1]. Figure 9 displays the

pattern, which is dramatically different to the S-pattern and its variations [18, 28]. The proof of our main result below makes use of this curious arrangement to construct a fermion-qubit mapping with optimal average locality.

Theorem 1. (Minimising the average Pauli weight for fermionic lattice Hamiltonians) Given a system of $n = N^2$ fermionic modes arranged in a square $N \times N$ lattice $G_{\rm F}$, with hopping interactions between neighbouring modes, then the Mitchison-Durbin pattern $f_{\rm M}$ is a fermionic enumeration scheme that minimises the average Pauli weight of the hopping terms.

Proof. Proof in Section III C.
$$\square$$

Remark 1. Optimising the average Pauli weight depends on the edgesum value $C^1(f)$, therefore calculating the optimal fermionic enumeration scheme for an arbitrary fermionic mode graph $G_{\rm F}$ is NP-complete as discussed in Section II E.

Remark 2 details all known scenarios to date where the optimal fermionic enumeration scheme is solvable in $\mathsf{poly}(n)$ time.

Remark 2. (Solutions for other graph types $G_{\rm F}$.) If the Hamiltonian H is as defined in Theorem 1, and if $G_{\rm F}$ belongs to any of the graph families in Figure 7, then a classical computer can efficiently find an optimal fermionic enumeration scheme for H.

Corollary 1.1. Using the Mitchison-Durbin pattern $f_{\rm M}$ to enumerate a square-lattice fermionic system's hopping terms produces Pauli strings with an average weight of $\frac{1}{3}\left(4-\sqrt{2}\right)\approx 0.86$ times the corresponding average Pauli weight that the S-pattern $f_{\rm S}$ produces.

Proof. On an $N \times N$ lattice, the Mitchison-Durbin pattern $f_{\rm M}$ and the S-pattern $f_{\rm S}$ have edgesums

$$C^{1}(f_{S}) = N^{3} - N \tag{26}$$

$$C^{1}(f_{\rm M}) = N^{3} - xN^{2} + 2x^{2}N - \frac{2}{3}x^{3} + N^{2}$$

$$- xN - 2N + \frac{2}{3}x,$$
(27)

respectively (see Appendix VIA for the derivation of $C^1(f_{\rm S})$, and Section IIIC for the derivation of $C^1(f_{\rm M})$). In Equation 27, the value x is the closest integer to $N-\frac{1}{2}\sqrt{2N^2-2N+\frac{4}{3}}$ (proof in Section IIIC1). Using Equation 24 and the number of hopping terms |E|=2N(N-1), the average Pauli weights are

$$APV(f_{\rm S}) = \frac{1}{2}N + \frac{3}{2}$$
 (28)

and, for large N,

$$APV(f_{\rm M}) \approx \frac{1}{6}(4 - \sqrt{2})N + \frac{1}{12}(20 + \sqrt{2})$$
 (29)

$$= 0.43N + 1.78. (30)$$

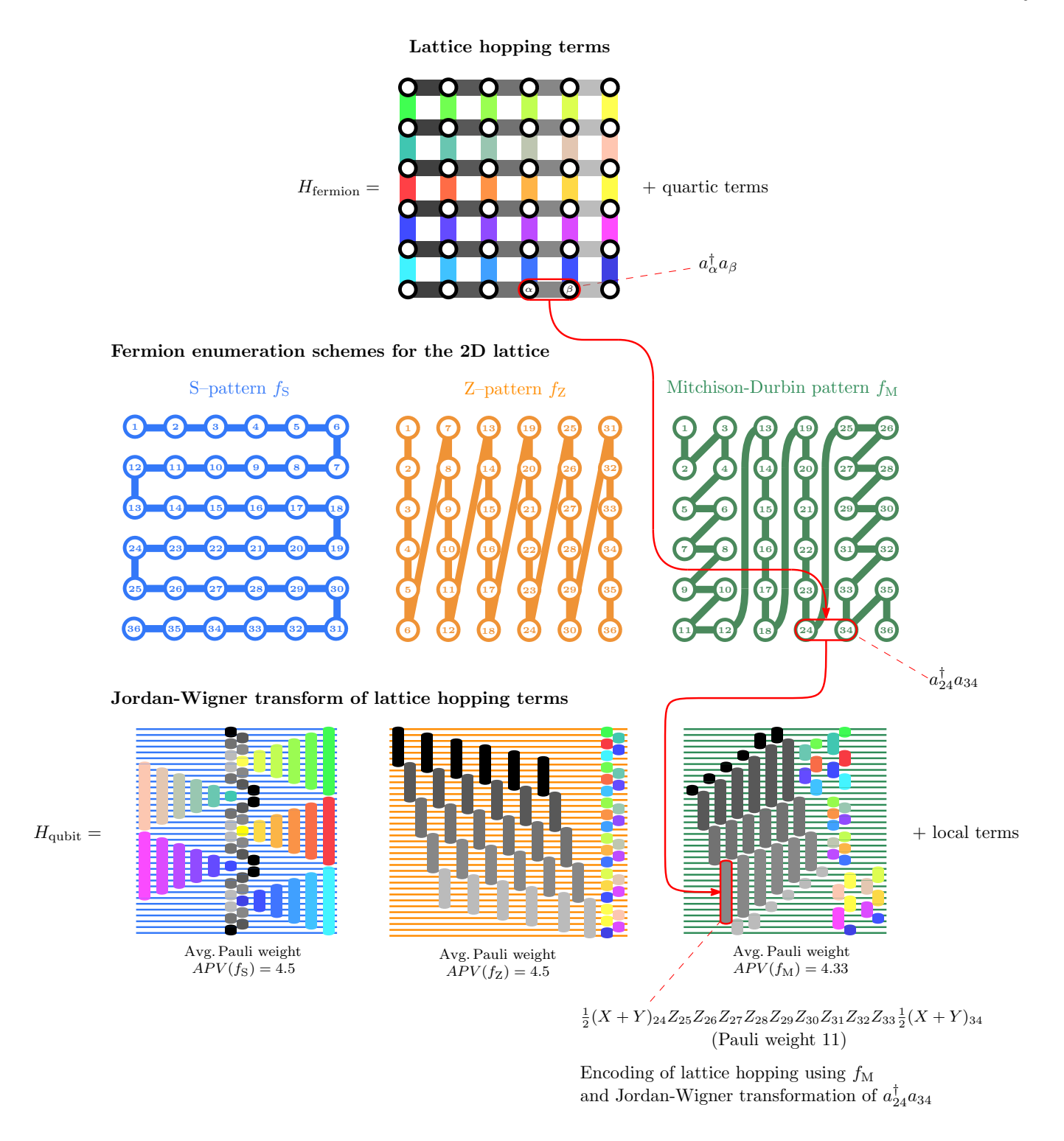


Figure 8: The Jordan-Wigner transformation produces different Pauli strings depending on the choice of enumeration scheme. Pauli strings correspond to the hopping term of the same colour in the 6×6 lattice at the top of the figure. On square lattices, the Mitchison-Durbin pattern produces Pauli strings of the lowest average weight.

Explicitly calculating the average Pauli weights for small N verifies that $APV(f_{\rm S}) > APV(f_{\rm M})$ for $N \geq 6$. The average Pauli weight is thus $APV(f_{\rm M})/APV(f_{\rm S}) \approx \frac{1}{3}(4-\sqrt{2}) \approx 0.86$ times what it was before changing from $f_{\rm S}$

to the $f_{\rm M}$ pattern.

We can conclude from Corollary 1.1 that, simply by labelling the fermions using the Mitchison-Durbin pattern rather than the S-pattern, we can produce a qubit

© 1986 Society for Industrial and Applied Mathematics

OPTIMAL NUMBERINGS OF AN N×N ARRAY* GRAEME MITCHISON† AND RICHARD DURBIN†

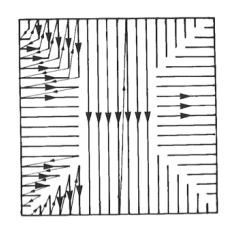




Figure 9: The original appearance of the Mitchison-Durbin pattern in their original paper [1], and Graeme Mitchison's sculpture of the optimal numbering of a 7×7 array. Reproduced with the permission of Richard Durbin.

Hamiltonian with terms that are 13.9% more local on average. This could immediately translate to a reduction by the same amount in the number of single-qubit measurements required in a VQE protocol. Even in the case of simulating small fermionic systems, this method provides a worthwhile advantage. For example, in Figure 8 where N=6, the ratio of the average Pauli weights using $f_{\rm M}$ and $f_{\rm S}$ is $4.33/4.5\approx 0.96$. That is, even for the 6×6 lattice, applying Theorem 1 could reduce the number of VQE measurements by 4%.

For $2 \leq N \leq 100$, Figure 27 shows the resulting average Pauli weights of various enumeration schemes on $N \times N$ lattices. Even on small lattices, the Mitchison-Durbin pattern can yield a meaningful reduction: for N = 20, $C^1(f_{\rm M})/C^1(f_{\rm S}) = \frac{7140}{7980} \approx 89.5\%$.

C. Proof of Theorem 1

This section contains a more elaborate version of the original proof [1]. The Mitchison-Durbin pattern $f_{\rm M}$ solves the edgesum or minimum 1-sum problem for an $N\times N$ lattice. Thus, its optimality (once proved) directly implies that the pattern $f_{\rm M}$ is an optimal choice to minimise the average Pauli weight of a Jordan-Wigner mapping, and Theorem 1 follows as a consequence.

Let G = (V, E) be the $N \times N$ square lattice. Label each vertex $\alpha \in V$ by its position (μ, ν) on the lattice, where $\mu, \nu \in \{1, 2, \dots, N\}$. For example, the vertex in the top-left corner has label (1, 1) and the vertex in the bottom-right has label (N, N).

Given a square lattice vertex enumeration scheme $f:V \to \{1,2,\dots,N^2\}$, the cost function for the minimum

p-sum problem is then

$$(C^{p}(f))^{p} = \sum_{(\alpha,\beta)\in E} |f(\alpha) - f(\beta)|^{p}$$
(31)

$$= \sum_{(\mu,\nu)\in V} \left(\underbrace{\left| f(\mu+1,\nu) - f(\mu,\nu) \right|^p}_{\text{horizontal; 0 if } (\mu+1,\nu)\notin V} \right)$$
(32)

$$+\underbrace{\left|f(\mu,\nu+1)-f(\mu,\nu)\right|^p}_{\text{vertical; 0 if }(\mu,\nu+1)\notin V}\right).$$

Call an enumeration scheme f for the square lattice G horizontally ordered if $f(\mu, \nu+1) > f(\mu, \nu)$ for all vertices $(\mu, \nu) \in V$. Similarly, call f vertically ordered if $f(\mu + 1, \nu) > f(\mu, \nu)$ for all $(\mu, \nu) \in V$.

Proposition 1. Let $p \ge 1$. Given a vertex enumeration scheme $f: V \to \{1, 2, ..., N^2\}$ for the $N \times N$ square lattice, then there exists a horizontally and vertically ordered enumeration scheme g such that $C^p(g) \le C^p(f)$. That is, there exists an optimal enumeration scheme for the $N \times N$ square lattice which is horizontally and vertically ordered.

Proof. Let f be a vertex enumeration scheme for the square lattice. Consider the enumeration scheme f' which is horizontally ordered, but otherwise the same as f. Thus, each row of the enumerated lattice f'(G) contains the same set of indices as f(G), except that the indices are permuted so as to be in order of ascending value if they were not already. Call the process of replacing f with f' the horizontal ordering of f. Define the vertical ordering of f similarly. We will prove Proposition 1 via successively proving statements S1–S3 below:

S1. The action of horizontally ordering an enumeration scheme f never increases $C^p(f)$.

The following two claims prove S1:

<u>Claim:</u> The horizontal ordering of f will always decrease the horizontal contributions to $C^p(f)$ in Equation 32 if p > 1.

<u>Proof:</u> Suppose f is not horizontally ordered; for example, there may be a row of the enumerated lattice f(G) such as the one in the top diagram of Figure 10. The horizontal contributions to $C^p(f)$ from this row are

$$|j_{1} - j_{2}|^{p} + |j_{2} - j_{3}|^{p} + |j_{3} - j_{4}|^{p} + \dots + |j_{i-1} - j_{i}|^{p} + |j_{i} - j_{i+1}|^{p} + \dots + |j_{N-1} - j_{N}|^{p}.$$
(33)

Consider modifying f by rearranging the positions of j_{i+1} and j_i , as in the second diagram of Figure 10. The contributions to $C^p(f)$ would now be:

$$|j_{1} - j_{2}|^{p} + |j_{2} - j_{3}|^{p} + |j_{3} - j_{4}|^{p} + \dots + |j_{i-1} - j_{i+1}|^{p} + |j_{i+1} - j_{i}|^{p} + \dots + |j_{N-1} - j_{N}|^{p}.$$
(34)

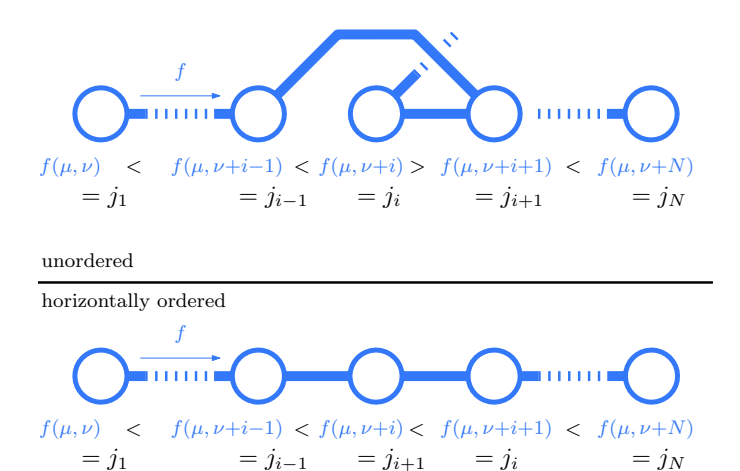


Figure 10: On a square lattice graph, horizontally ordering each row never increases the edgesum.

The difference in the horizontal contribution to $C^p(f)$ upon modifying f in this way is thus the difference between Equations 34 and 33. This value is $|j_{i-1} - j_{i+1}|^p - |j_{i-1} - j_i|^p < 0$ if $p \ge 1$ because $j_{i+1} < j_i$.

The action of horizontally ordering f is simply a chain of as many swaps of the above form as is necessary to leave the vertices in each row of the lattice in ascending order. Thus, horizontally ordering f will always decrease the horizontal contributions to $C^p(f)$ if $p \geq 1$.

<u>Claim</u>: The horizontal ordering of f will never increase the vertical contributions to $C^p(f)$ in Equation 32 if $p \ge 1$.

<u>Proof:</u> (Use Figure 11 as a guide.) Suppose that f is not horizontally ordered. Vertical contributions to $C^p(f)$ will change upon the horizontal ordering of f if the process affects adjacent rows differently. This occurs if there exist vertices (μ, ν) and $(\mu, \nu + 1)$ which are horizontally ordered with $f(\mu, \nu) = i < f(\mu, \nu + 1) = j$, and if vertices $(\mu + 1, \nu)$ and $(\mu + 1, \nu + 1)$ are not, with $f(\mu + 1, \nu) = m > f(\mu + 1, \nu + 1) = n$.

Initially, the vertical contributions to $C^p(f)$ from these four vertices is

$$|i - m|^p + |j - n|^p$$
. (35)

Because i < j and m > n, the values (i - m) and (j - n) in Equation 35 are unequal. Consider modifying f by rearranging the positions of m and n, as in Figure 11. The new vertical contributions are

$$|i-n|^p + |j-m|^p$$
. (36)

The values of (i-n) and (j-m) may not be equal, but they are closer in value to each other than the values (i-m) and (j-n) were. For p>1, if a+b is constant then a^p+b^p reduces in value the

closer a and b are to each other. Therefore, the vertical contributions to $C^p(f)$ in Equation 36 are less than the vertical contributions in Equation 35. If p = 1, the contributions are unchanged by the modification. This proves the claim.

S2. The action of vertically ordering a horizontally ordered enumeration scheme f preserves its horizontal ordering.

Suppose that f is a horizontally ordered enumeration scheme. This claim proves S2:

 $\underline{\text{Claim:}}$ The vertical ordering of f preserves the horizontal ordering.

<u>Proof:</u> (Use Figure 12 as a guide.) Let g be the vertically ordered version of f, and suppose that it is not horizontally ordered. Then there must be a pair of vertices (μ, ν) and $(\mu, \nu') \in V$ in the lattice such that $g(\mu, \nu) = k < g(\mu, \nu')$ and $\nu' < \nu$, for $k \in \{1, 2, \dots, N^2\}$.

The enumeration scheme g is vertically ordered: therefore, each of the $\mu-1$ vertices above (μ,ν) must have a value less than $g(\mu,\nu)=k$. Because the vertex with label k is on the same row as (μ',ν) , then each of the $\mu-1$ vertices above (μ,ν') must also have a value less than k.

Now consider the original enumeration scheme f, before vertical ordering. The vertex with label k is in the same column of the lattice as it was under g, i.e. column ν . Let this vertex be (μ', ν) ; then $f(\mu', \nu) = k$. Because g is just a vertical ordering of f, there must still be $\mu - 1$ vertices in columns ν and ν' with label less than k, and because f is horizontally ordered then every vertex to the left of these $\mu - 1$ vertices has a label with value less than k. But every vertex to the left of (μ', ν) must also have a label with value less than k, as $f(\mu', \nu) = k$. Therefore, under the enumeration scheme f, any column to the left of column ν contains $(\mu - 1) + 1$

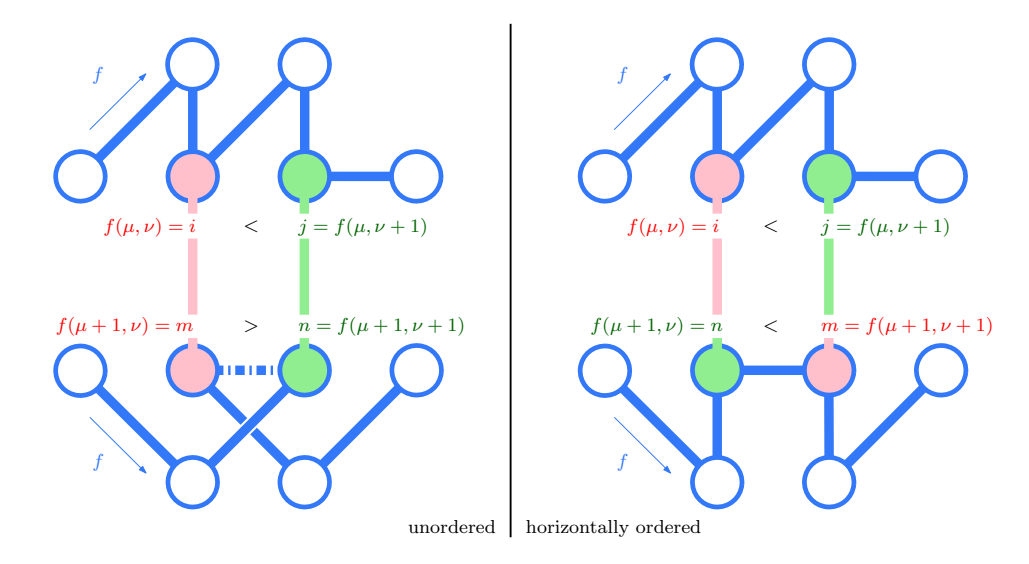


Figure 11: On a square lattice graph, the action of horizontally ordering a vertex enumeration scheme f never increases the vertical contributions to $C^p(f)$.

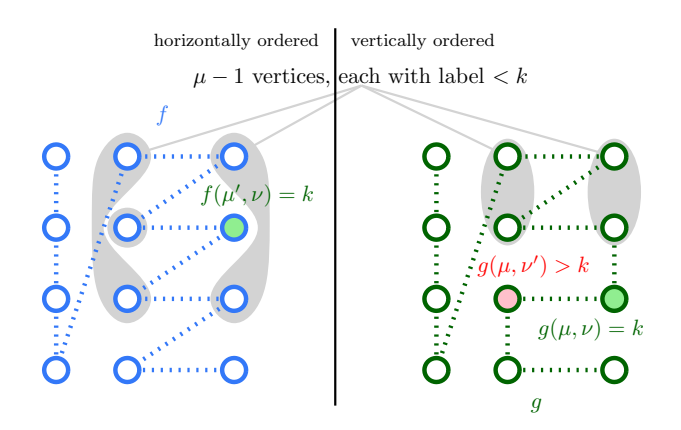


Figure 12: If a vertex enumeration scheme f is horizontally ordered, then its vertical ordering g must also be horizontally ordered. This figure shows the contradiction that would arise if this were not the case.

 $1 = \mu$ vertices with labels of value less than k. But we know that column ν' contains exactly $\mu - 1$ vertices with label less than k, and $\nu' < \nu$. This is a contradiction.

S3. For every vertex enumeration scheme f there exists a horizontally and vertically ordered scheme g with $C^p(g) \leq C^p(f)$.

This results from combining statements S1 and S2.

This proves Proposition 1.

Proposition 1 informs the discussion of numeric results when p>1 in Section III E. However, from this point the proof of Theorem 1 only concerns the minimum 1-sum problem, for which p=1. Every enumeration scheme referenced from hereon is horizontally and vertically or-

dered. The following result greatly simplifies the calculation of $C^1(f)$:

<u>Claim:</u> Let V_1, V_r, V_t, V_b be the vertices in the left column, right column, top row and bottom row of the square lattice, respectively. Given a horizontally and vertically ordered vertex enumeration scheme $f: V \to \{1, 2, \dots, N^2\}$ for the lattice, the cost function for the minimum 1-sum problem is

$$C^{1}(f) = \sum_{\alpha \in V_{b}} f(\alpha) + \sum_{\alpha \in V_{r}} f(\alpha) - \sum_{\alpha \in V_{l}} f(\alpha) - \sum_{\alpha \in V_{t}} f(\alpha).$$
(37)

<u>Proof:</u> As f is horizontally and vertically ordered, Equation 32 becomes

$$C^{1}(f) = \sum_{(\mu,\nu)\in V} \left(f(\mu+1,\nu) + f(\mu,\nu+1) - 2f(\mu,\nu) \right)$$

$$= 2f(N,N) + \sum_{\mu=2}^{N-1} f(\mu,N) + \sum_{\nu=2}^{N-1} f(N,\nu)$$

$$- \sum_{\mu=2}^{N-1} f(\mu,1) - \sum_{\nu=2}^{N-1} f(1,\nu) - 2f(1,1)$$

$$= \sum_{\alpha\in V_{b}} f(\alpha) + \sum_{\alpha\in V_{r}} f(\alpha) - \sum_{\alpha\in V_{l}} f(\alpha) - \sum_{\alpha\in V_{t}} f(\alpha) .$$

$$(40)$$

Any horizontally and vertically ordered enumeration scheme f must begin at a corner of the square lattice and end at the opposite corner. Assume without loss of generality that f(1,1) = 1 and $f(N,N) = N^2$, and that

f(N,1) < f(1,N). As in Figure 13, let U be the section of the lattice that f labels up to (N,1), and let V be the section of the lattice that it labels from (1,N) onwards. Because f can never "double back" on itself without violating horizontal or vertical ordering, the regions U and V are upper- and lower- skew block-triangular sections of the lattice, respectively.

Define S(U) and S(V) to be the sums of the labels of vertices on the boundary of the lattice in the regions U and V, respectively. By Equation 37, these S quantities completely determine the contributions to $C^1(f)$ from the vertices in U and V. Suppose that U and V are fixed regions, and that the goal is to choose an enumeration scheme f to maximise S(U) and minimise S(V). Lemma 2 provides a strategy to solve this problem.

Lemma 2. Let U and V be upper- and lower- skew block-triangular regions of the $N \times N$ square lattice, containing vertices (N,1) and (1,N) respectively, as above. For any enumeration scheme $f: V \to \{1,2,\ldots,N^2\}$ that labels the vertices in U before any outside of U, and labels the vertices in V after any outside of V, define S(U) and S(V) to be the sums of the labels on the lattice boundaries of U and V, respectively. Then, the rules below construct a horizontally and vertically ordered enumeration scheme f that yields the maximum value for S(U):

- a) Fill each new column/row as far as possible while preserving horizontal and vertical ordering;
- b) After filling a column/row as far as possible, begin to fill the longest remaining column/row that remains, starting from the top-leftmost available vertex of the lattice.

By symmetry, the reverse of this process provides a scheme that yields the minimum value for S(V).

Proof. (For reference, Figure 13 provides one example each of ordered enumeration schemes that do and do not satisfy the rules in Lemma 2.)

For a): if f did not fill a row as far as possible, then the first label on the subsequent column would be less than if f had filled the initial row, as Figure 14 demonstrates. Only the first entries of each row and column contributing to S(U), so this is not an optimal result.

For b): suppose that, beginning at index i, the enumeration scheme f fills a column of length a before it fills a row of length b > a, as in Figure 15. Then the contribution of the row and column to S(U) is i+(i+a). However, following rule b) in Lemma 2 would mean filling the row before the column, and the contribution to S(U) would be i+(i+b)>i+(i+a). Therefore, optimal enumeration schemes must follow rule b) as well as rule a).

Note that rules a) and b) describe a unique enumeration scheme for U, and so it is not possible to prescribe any further rules. Thus the resulting enumeration scheme must maximise S(U).

Corollary 2.1. The consequence of the rules in Lemma 2 is that an enumeration scheme f that minimises $C^1(f)$ must:

- a) Fill the largest square that lies in U by alternating between successively longer rows and columns, before filling the remaining columns and rows of U that are outside the square in order of decreasing length (a detail that the rightmost diagrams in Figures 13 and 15 include);
- b) Fill $\overline{U \cap V}$, the region between U and V, with columns from top-to-bottom. This ensures that labels with the least possible value occupy the bottom row of the lattice outside V, and that labels with the greatest possible value occupy the top row of the lattice outside U.

<u>Proof:</u> Given Lemma 2, Corollary 2.1 is self-evident. Figure 13 illustrates Corollary 2.1 b).

Lemma 2 showed how to minimise C(f) for fixed shapes of the regions U and V; Lemmas 3 and 4 will show which shapes of U and V can give a global minimum for $C^1(f)$.

Lemma 3. Let U and V be regions of the $N\times N$ square lattice that satisfy Lemma 2's conditions, and let f be an optimal enumeration scheme that follows the rules of Lemma 2. Then, delete from U the region to the right of the largest square in U, and add it to $\overline{U\cap V}$. Similarly, delete from V the region to the left of the largest square in V, and add it to $\overline{U\cap V}$. This reduces $C^1(f)$.

Proof. Define E_1 to be sum of the labels of the topmost vertices in U that are to the right of the largest square in U, E_2 to be the sum of the labels of the leftmost vertices beneath the largest square in U, and E_3 to be the sum of the labels of the topmost vertices outside of U. Define F_1 , F_2 and F_3 analogously, as in Figure 16. Then,

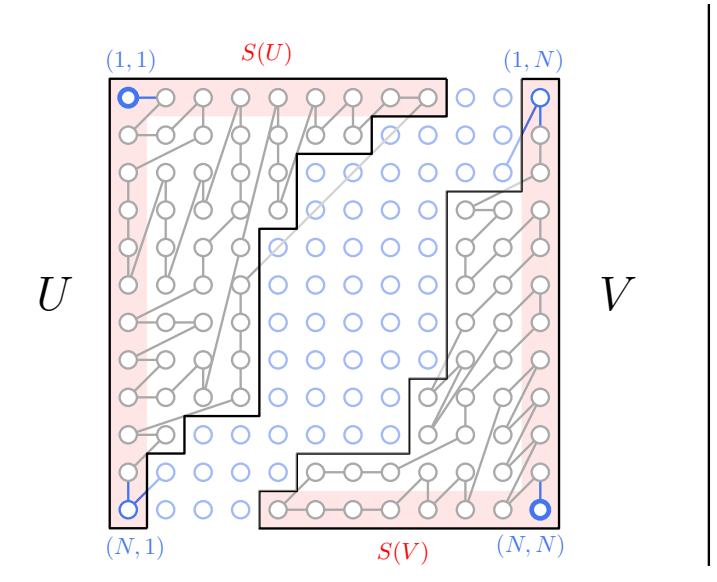
$$C^{1}(f) = (F_1 + F_2 + F_3) - (E_1 + E_2 + E_3)$$
 (41)
+ labels of edge vertices in squares.

Any horizontally and vertically ordered enumeration scheme that follows the rules of Lemma 2 must label the vertices in the largest squares of U and V first and last. Therefore, the deletion operation in Lemma 3's statement does not change the labels of the edge vertices in the squares.

<u>Claim:</u> The deletion operation in Lemma 3 increases $(E_1 + E_2 + E_3)$.

<u>Proof:</u> The following three steps implement the deletion operation in Lemma 3.

- 1. Delete from V the region to the left of the largest square in V, and add it to $\overline{U \cap V}$. This increases E_3 and leaves E_1 and E_2 unchanged.
- 2. Delete the rightmost column from U, and add it to $\overline{U \cap V}$. As in Figure 17, let x be the side length of the largest square in U, let w be the height of the



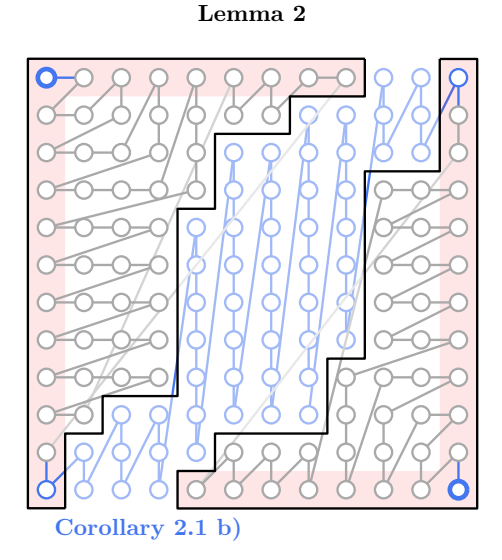


Figure 13: **Left:** An example of the regions U and V, and an ordered enumeration scheme that does not follow the rules in Lemma 2. Vertices on the boundaries of U and V contribute to S(U) and S(V). **Right:** An example of an enumeration scheme that follows the rules in Lemma 2 and hence maximises S(U) and minimises S(V). The scheme fills the space between U and V with vertical columns as a consequence, via Corollary 2.1 b).

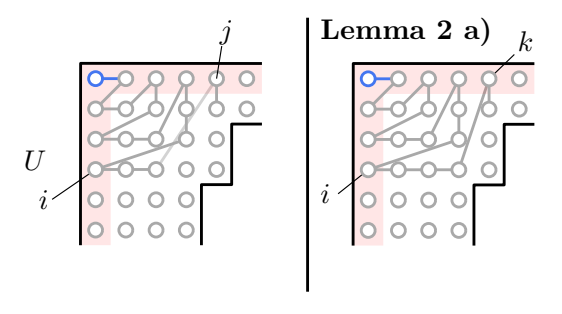


Figure 14: **Left:** An enumeration scheme that does not fill the row containing label i as far as possible. **Right:** The enumeration scheme now fills the row containing i as far as possible whilst preserving horizontal and vertical ordering. It is clear that k > j.

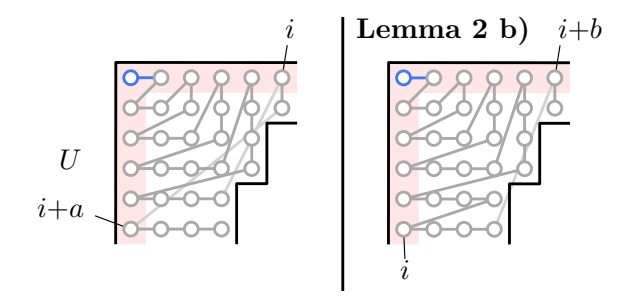


Figure 15: **Left:** An enumeration scheme that does not fill rows and columns in order of decreasing length. **Right:** The enumeration scheme now fills the row of length b before the column of length a < b. It is clear that i + (i + b) > i + (i + a).

rightmost column of U and let h be the height of the bottommost row of U with length greater than w. This step reduces the labels of the bottommost h elements in E_2 by w, and so E_2 decreases by hw. Meanwhile, the value of E_1 increases because of the new label for the topmost vertex of the column that has joined $\overline{U} \cap \overline{V}$. The label of this vertex increases by at least hx, and so the value of $E_1 + E_2$ increases by hx - hw = h(x - w) > 0, as x > w.

3. Repeat step 2 until the entire region in U to the right of the largest square in U has joined $\overline{U \cap V}$. Breaking down the deletion operation in this way reveals that $E_1 + E_2 + E_3$ increases.

By symmetry, the deletion operation must therefore decrease $F_1+F_2+F_3$, and so $C^1(f)$ decreases overall. \square

Lemma 4 shows how to structure the regions outside the largest squares in U and V to give the least value for $C^1(f)$.

Lemma 4. Let U and V be regions of the $N \times N$ square lattice that satisfy Lemma 3's conditions, and let f be an optimal enumeration scheme that follows the rules of Lemma 2. Suppose the side length of the largest square in U is x. Then, modify U by imposing a length of x on all rows down to a height x above the bottom row, and then give the row at height y < x a length of y or y - 1. Perform the inverse modification to V.

For fixed x, the resulting optimal enumeration scheme with these new U and V yields the minimum $C^1(f)$ over all possible enumeration schemes for the square lattice.

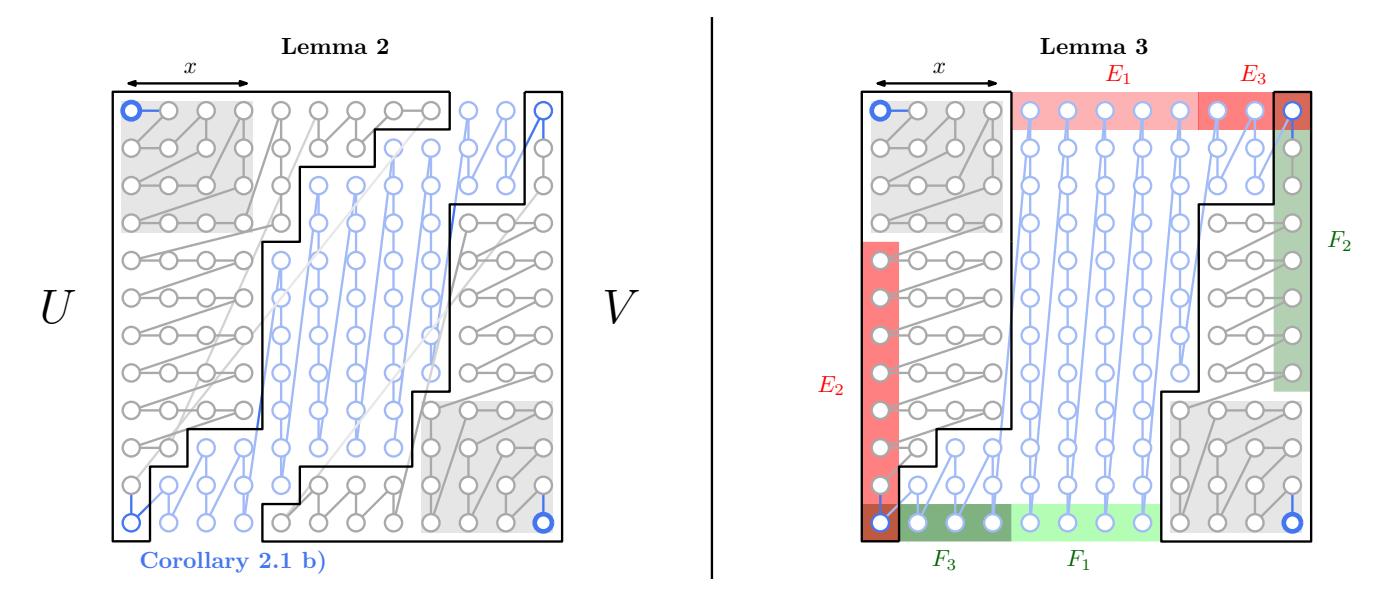


Figure 16: Lemma 3 shows how to delete regions of U and V so that the new enumeration scheme has a smaller edgesum C^1 .

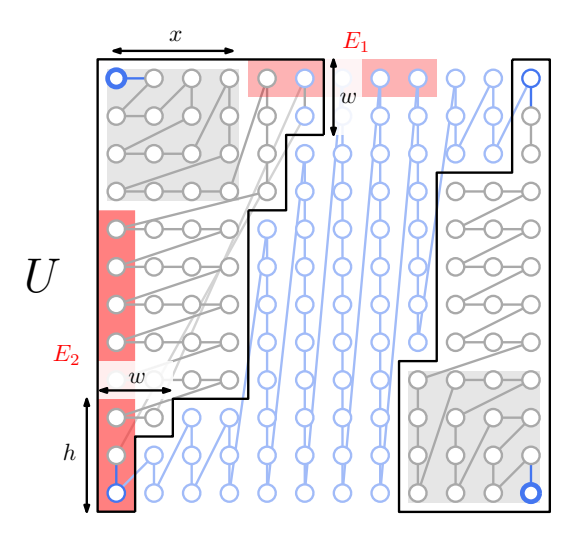


Figure 17: Deleting the rightmost column of U increases the value of $E_1 + E_2$.

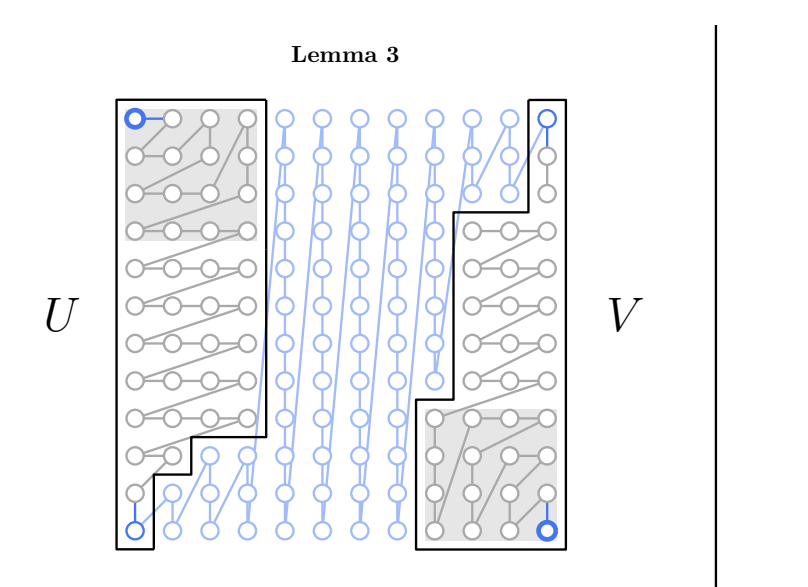
Proof. As in Figure 19, take a row of U outside of the top-left square. Let it be the yth row from the bottom, and let its length be w. Then, if w < y, increase the row's length to w+1. This increases by +1 the labels of the y-1 bottommost vertices in the left-hand column of the lattice. Similarly, the labels of the w leftmost vertices in the bottom row increase by w0. With this modification to the enumeration scheme w1, the value of w2 changes by w3 changes by w4 changes by w6.

If w>y, decrease the row's length to w-1. This subtracts 1 from the labels of the y-1 bottommost vertices in the left-hand column of the lattice, and from the labels of the w-1 leftmost vertices in the bottom row. Thus the value of $C^1(f)$ changes by $-((w-1)-(y-1)) \le 0$, i.e. it decreases by $w-y \ge 0$.

By symmetry, the inverse process works on V. Repeated application of these steps thus minimises $C^1(f)$; Figure 18 shows the end result.

Finally, only one degree of freedom remains in choosing the shape of U: the side length x of its largest square. Lemma 5 expresses the edgesum of the pattern as a function of N and x. Corollary 5.1 then provides the optimal value for x and hence the Mitchison-Durbin pattern $f_{\rm M}$

Lemma 5. Let U and V be regions of the $N \times N$ square lattice that satisfy Lemma 4's conditions, and let f be an optimal enumeration scheme that follows the rules of Lemma 2. Suppose that the side lengths of the largest squares in U and V are both x. Then the edgesum of f



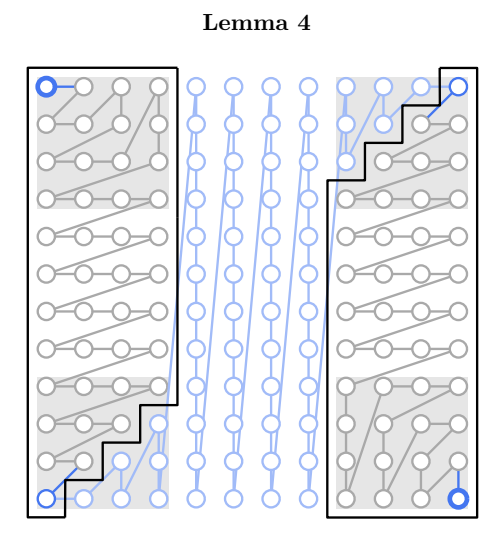


Figure 18: Lemma 4 shows the optimal shape for regions U and V in order to minimise the edgesum C^1 . The resulting pattern is the Mitchison-Durbin pattern f_M .

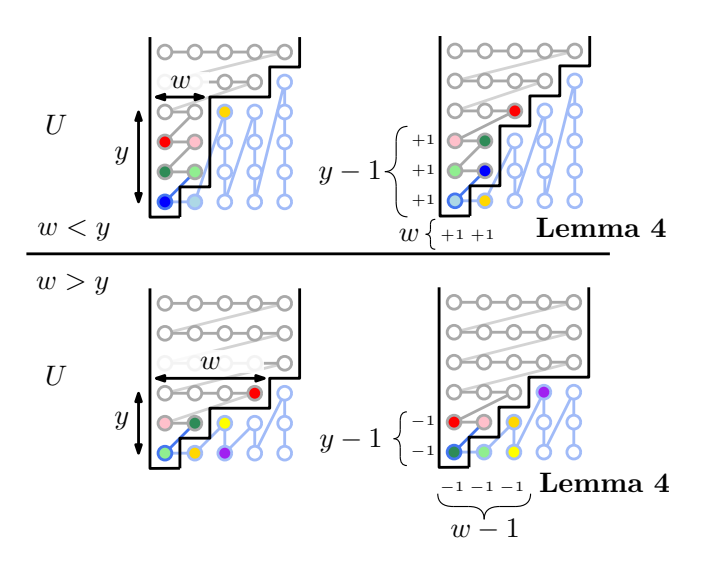


Figure 19: Modifying the shape of U in Lemma 4 to reduce the edge sum $\mathbb{C}^1.$

is

$$C^{1}(f_{\rm M}) = N^{3} - xN^{2} + 2x^{2}N - \frac{2}{3}x^{3} + N^{2}$$

$$-xN - 2N + \frac{2}{3}x.$$
(42)

Proof. See Section III C 1.

Corollary 5.1. For $N \geq 5$, the value of x that minimises $C^1(f)$ in Equation 42 is $x = N - \frac{1}{2}\sqrt{2N^2 - 2N + \frac{4}{3}}$. Round x to the nearest integer to obtain the minimum $C^1(f)$ over all enumeration schemes for the $N \times N$ square lattice.

Proof. Treat
$$N$$
 and x as continuous variables, and use calculus to find that minimum of $C^1(f)$ in Equation 42 occurs when $x = N - \frac{1}{2}\sqrt{2N^2 - 2N + \frac{4}{3}}$.

Note that the optimal value for x in Corollary 5.1 is a refinement on the value that Mitchison and Durbin give in [1]: they use the approximation $x=\left(1-\frac{1}{\sqrt{2}}\right)N$. For all intents and purposes, these values are extremely close and rounding this approximate value for x gives the same integer as $N-\frac{1}{2}\sqrt{2N^2-2N+\frac{4}{3}}$ for most values of N.

Define the Mitchison-Durbin pattern $f_{\rm M}$ to be any of the optimal enumeration schemes that fill region U first and region V last, where the value of N completely determines U and V via the successive restrictions of Lemmas 2–5 and Corollary 5.1. For example, in Figure 8, N=6 and x=2. In Figure 20, N=17 and x=5. This completes the proof.

1. Edgesum of the Mitchison-Durbin pattern

This section calculates the edge sum of the enumeration pattern f in Lemma 5. Divide the enumeration pattern on the $N\times N$ grid up into regions A,B,\ldots,G as in Figure 20. Let the label of each region also denote its edge sum. Therefore

$$C^{1}(f) = A + B + C + D + E + F + G$$

$$+ AB + AD + BD + BC + CD$$

$$+ DE + EF + DF + FG + DG.$$
(43)

where AB, \ldots, DG denote the sums of the differences between vertex labels across the interfaces between each

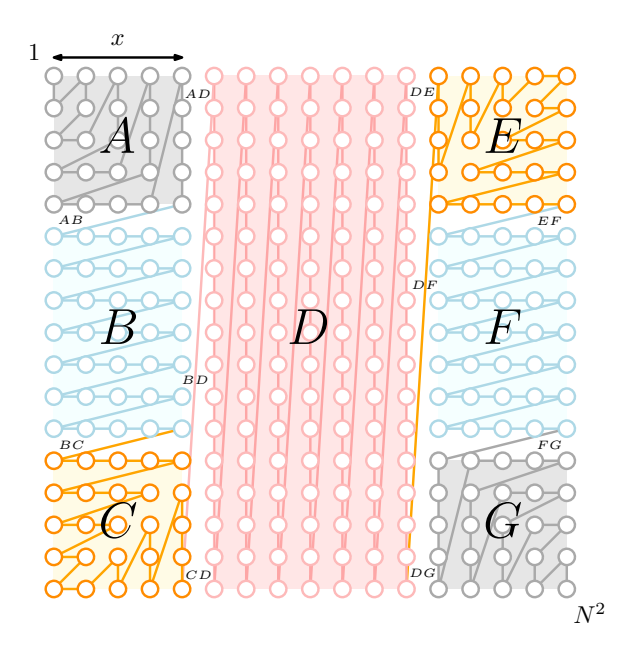


Figure 20: Sections of the $N \times N$ square lattice and an enumeration pattern f that satisfies Lemma 4.

pair of regions. Due to the symmetry of f, Equation 43 becomes

$$C^{1}(f) = 2(A + B + C) + D$$

$$+ 2(AB + AD + BC + BD + CD).$$
(44)

We can derive expressions for the contributions of each region to $C^1(f)$ by observing the patterns in the differences betwen vertex labels. Figure 21 shows the progression of vertex labels in regions A–D of the square lattice. Within each of these regions, the enumeration scheme is horizontally and vertically ordered. Thus, using Equation 37 on region A gives:

$$A = \left(\sum_{k=0}^{x-2} (x(x-2) + 2 + k) + \sum_{j=1}^{x} (x(x-1) + j)\right)$$
$$-\left(\sum_{k=1}^{x} (k(k-1) + 1) + \sum_{j=1}^{x} (j(j-2) + 2)\right) \quad (45)$$
$$= \frac{1}{6}(x-1)(6 + x(8x-1)). \quad (46)$$

The other regions contribute the following quantities:

$$B = (N - 2x)(x - 1) + x^{2}(N - 2x - 1)$$
 (47)

$$C = \frac{1}{6}(x-1)(6+x(8x-1)) \tag{48}$$

$$D = N^3 - 2xN^2 - 2xN + 2x - N. (49)$$

The vertex labels in Figure 21 also make it simple to calculate the contributions to $C^1(f)$ from the interfaces

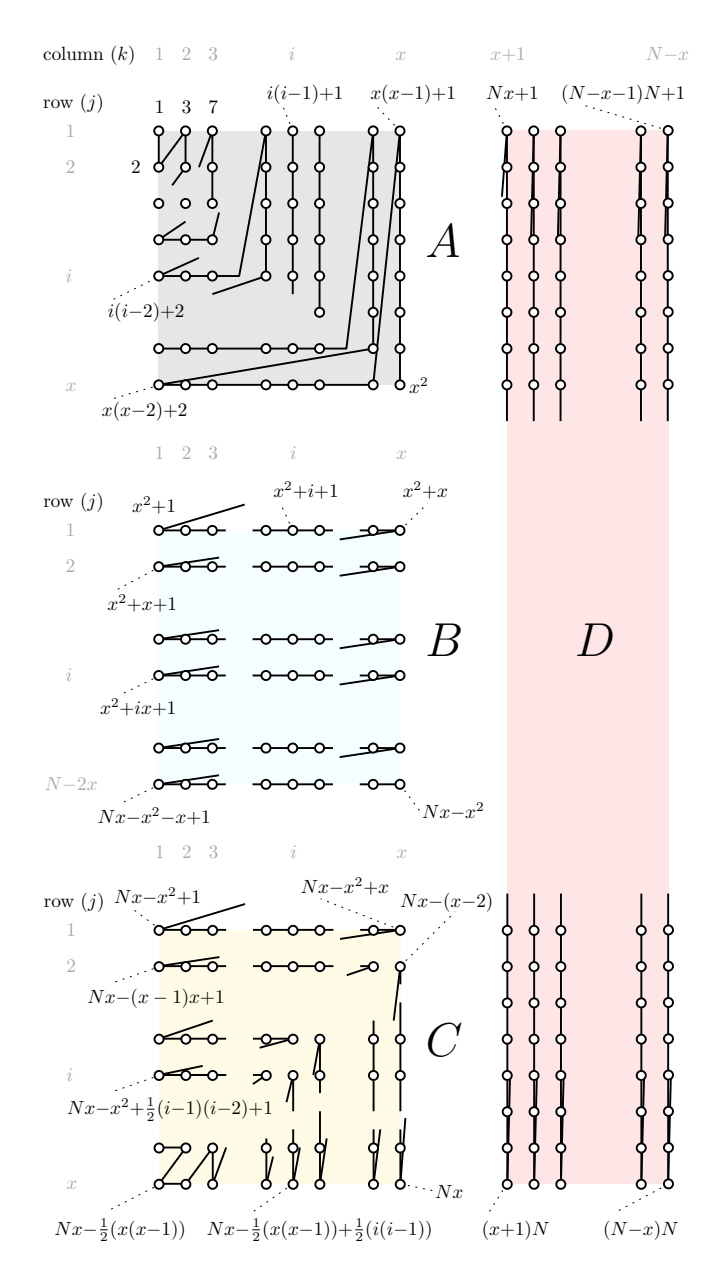


Figure 21: An in-depth look at the Mitchison-Durbin pattern $f_{\rm M}$. Vertex labels indicate the position of each vertex in the enumeration scheme.

between the regions:

$$AD = \sum_{j=1}^{x} \left((x(x-1) + j) - (Nx + j) \right)$$
 (50)

$$= Nx^2 - x^3 + x^2 (51)$$

$$AB = 1 - 2x + 2x^2 (52)$$

$$BD = \frac{1}{2} \left(N^2 + N - 3xN + xN^2 + 2x^2 - 2x - 2x^2 N \right)$$
(53)

$$BC = x^2 (54)$$

$$CD = 1 - 2x + xN + x^2. (55)$$

Substituting Equations 46–55 into Equation 44 gives the result,

$$C^{1}(f_{\rm M}) = N^{3} - xN^{2} + 2x^{2}N - \frac{2}{3}x^{3} + N^{2}$$

$$-xN - 2N + \frac{2}{3}x.$$
(56)

D. Reducing the average Pauli weight for cellular fermionic lattices

Theorem 1 reduces the average Pauli depth of qubit Hamiltonians by making judicious use of the solutions to the edgesum problem. As Remark 2 discusses, there are only a handful of other graph families for which edgesum solutions are known. It is tempting to think that there is not much use our approach if the fermionic interaction graph $G_{\rm F}$ does not belong to one of these families. In this section, however, we show an example graph for which a "common-sense" approach to constructing a good enumeration scheme can provide an order-of-magnitude reduction in its edgesum and hence in average Pauli weight.

Consider fermions interacting between modes in an $(n \times n) \times (N \times N)$ cellular arrangement of square lattices, where each $n \times n$ sub-lattice connects to adjacent sub-lattices via a single edge. Here we use the cellular pattern in Figure 22, where the connections are from each $n \times n$ lattice's top left vertex to the two closest vertices from neighbouring lattices.

It is possible to enumerate the fermionic modes on a cellular arrangement graph with the Z–pattern $f_{\rm Z}$ or the S–pattern $f_{\rm S}$ from Section III B, treating the whole graph as a single square lattice. As Figure 22 shows, another way of enumerating the modes is to enumerate each sublattice locally before moving on to the next, progressing through the entire graph via an S– or Z–pattern. We call these two enumeration procedures $f_{\rm S'}$ and $f_{\rm Z'}$, respectively.

The edgesums of these schemes on the cellular arrange-

ment graph are:

$$C^{1}(f_{S}) = \begin{cases} (Nn)^{3} - Nn - N(N-1)(n-1) \\ -\sum_{k=0}^{N-1} \sum_{i=kn+2}^{(k+1)n} (2i-1), & n \text{ even} \\ (Nn)^{3} - Nn - N(N-1)(n-1) \\ -\sum_{k=0}^{N-1} \sum_{i=kn+1}^{(k+1)n-1} (2i-1), & n \text{ odd,} \end{cases}$$

(57)

$$C^{1}(f_{\rm Z}) = (Nn)^{3} - Nn - N(N-1)(n-1)$$

$$- nN^{2}(n-1)(N-1),$$
(58)

$$C^{1}(f_{Z'}) = \begin{cases} N^{3}n^{2} + n^{3}N^{2} - n^{2}N^{2} \\ -2nN^{2} - n^{2}N + 2N^{2} \\ +2nN + n^{2} - 2N - n, & n \text{ even} \\ N^{3}n^{2} + n^{3}N^{2} - n^{2}N^{2} \\ -nN^{2} - n^{2}N + N^{2} \\ +2nN + n^{2} - 2N - 2n + 1, & n \text{ odd,} \end{cases}$$

$$(59)$$

and while the value of $C^1(f_{S'})$ also depends on the parities of n and N, it is strictly greater than $C^1(f_{Z'})$.

By using $f_{Z'}$ rather than f_{Z} , the edgesum of a large cellular arrengement graph reduces by an order of magnitude:

$$\lim_{N \to \infty} \frac{C^1(f_{Z'})}{C^1(f_Z)} = \frac{n^2}{n^3 - n^2 + n} = \mathcal{O}\left(\frac{1}{n}\right); \tag{60}$$

$$\lim_{n \to \infty} \frac{C^1(f_{Z'})}{C^1(f_Z)} = \frac{1}{N} \,. \tag{61}$$

If $n = \mathcal{O}(N)$, then the graph has $\mathcal{O}(N^4)$ vertices. From choosing $f_{Z'}$ rather than f_Z , the $\mathcal{O}(1/N)$ factor reduction in edgesum is thus proportional to the fourth root of the number of vertices. This is a much more striking improvement than the constant-factor improvement that Corollary 1.1 proffers, even though we have not proved that $f_{Z'}$ is an optimal enumeration scheme for the cellular arrangement graph.

E. Reducing the average pth power of Pauli weight for a square lattice

In Section III A, we introduced other figures of merit for fermionic enumeration schemes, such as the average pth power of Pauli weight for p > 1. For a given fermionic mode graph $G_{\rm F}$, this corresponds to finding an enumeration scheme f that minimises the p-sum

$$C^{p}(f) = \left(\sum_{(u,v)\in E} |f(u) - f(v)|^{p}\right)^{1/p}.$$
 (62)

The p=1 case is the edge sum problem and via Remark 1 is NP-complete. George and Pothen showed that the minimum 2-sum problem is also NP-complete [44].

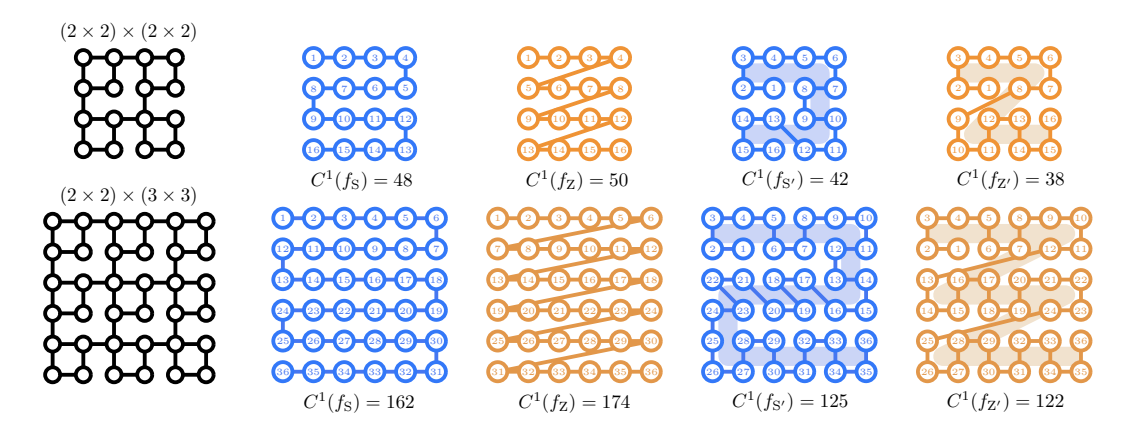


Figure 22: Edgesums for some enumeration schemes of $(n \times n) \times (N \times N)$ cellular arrangement patterns.

Enumeration scheme f	$C^1(f)$	$C^p(f), p > 1$	
Mitchison-Durbin pattern $f_{\rm M}$	$N^{3} - xN^{2} + 2x^{2}N - 2x^{3}/3 + N^{2} - xN - 2N + 2x/3$	Includes terms $\geq \sim 2x^{p+1}N^p \sim 2k^{p+1}N^{2p+1}$ where $x = kN$	
S-pattern $f_{\rm S}$	$N^3 - N$	$(N-1)\left(\sum_{k=1}^{N-1} (2k+1)^p + N + 1\right) \sim \frac{2^p}{p+1} N^{p+2} + \mathcal{O}(N^{p+1})$	
Z-pattern $f_{\rm Z}$	$N^3 - N$	$(N-1)(N^{1+p}+N) = N^{p+2} - N^{p+1} + N^2 - N$	
Diagonal pattern $f_{\rm D}$	$4N^3/3 - N^2 - N/3$	$2\left(\sum_{k=1}^{N-2} (2k+1)(k+1)^p + (N-1)N^p + 1\right) = \sim \frac{4}{p+2}N^{p+2} + \mathcal{O}(N^{p+1})$	
		Theoretical limit $\sim \frac{4}{2^p(p+2)}N^{p+2} + \text{smaller}$	

Figure 23: Results for the minimum p-sum problem for the square lattice for $p \ge 1$. While the Mitchison-Durbin pattern $f_{\rm M}$ minimises $C^p(f)$ for p = 1, it performs the worst of all the options for p > 1. The diagonal pattern $f_{\rm D}$ performs better than the rest for p > 2.

They develop spectral approaches to solving the minimum 1-sum and 2-sum problems for any graph $G_{\rm F}$. Separately, Mitchison and Durbin [1] explore the minimum p-sum problem where the graph $G_{\rm F}$ is a square lattice, and conclude with Proposition 2:

Proposition 2. (Mitchison and Durbin's results for the minimum p-sum problem on an $N \times N$ lattice [1]) Given a system of $n = N^2$ fermionic modes arranged in a square $N \times N$ lattice G_F , with hopping interactions between neighbouring modes, the following are the lower limits for the value of $C^p(f)$:

- (a) If 0 , then there exists an enumeration scheme <math>f with $C^p(f) = \mathcal{O}(N^2)$.
- (b) If $\frac{1}{2} , then <math>C^p(f) \ge \frac{1}{2p+1}N^{1+2p} + \mathcal{O}(N^{2p})$.
- (c) If p = 1, then f_M gives the minimum value as shown in Theorem 1.

(d) If
$$p > 1$$
, then $C^p(f) \ge \frac{4}{2^p(p+2)}N^{p+2}$.

The lower bounds in (b) and (d) are theoretical limits, and to date there are no known enumeration schemes that achieve their low coefficients. However, the "diagonal pattern" f_D has edgesum

$$C(f_{\rm D}) \approx \frac{4}{p+2} N^{p+2} + \mathcal{O}(N^{p+1}),$$
 (63)

which has the same order of magnitude in N as the theoretical limit in (d).

Proof. See Propositions 2–4 of [1].
$$\Box$$

Remark 3. (Best known results for the minimum p-sum problem on a square lattice, $p \ge 1$)

Figure 23 provides a table of known results for four enumeration schemes $f_{\rm S}$, $f_{\rm M}$, $f_{\rm Z}$, and $f_{\rm D}$ (the diagonal pattern) in the regimes p=1 and p>1. The diagonal pattern is the solution to the bandwidth problem (from

Section II E) on rectangles [1], and is the best-performing pattern for the minimum p-sum problem for $p>1,\ N\to\infty$.

IV. IMPROVING BEYOND OPTIMALITY WITH ANCILLA QUBITS

All of the techniques in Section III have permitted only as many qubits as there are fermionic modes. Theorem 1, for example, details the optimal Jordan-Wigner mapping for the task if one is restricted to using N^2 qubits to simulate an $N \times N$ fermionic lattice. However, permitting m > n qubits, there is a competitive interplay between the qubit count of a fermion-qubit mapping and the locality of its Hamiltonian. As qubits are costly with current technology, the qubit-locality tradeoff begs the question: what is the maximum benefit a mapping could gain by using an extra one or two qubits?

Moll et al. [49] show how to reduce the number of qubits in a Jordan-Wigner mapping at the cost of introducing more terms into the molecular Hamiltonian. Auxiliary qubit mappings [18, 28, 34, 35, 50] show the converse: that by introducing more qubits into a simulation it is possible to vastly simplify the Hamiltonian. Verstraete and Cirac showed that a system combining an $N \times N$ 2D qubit lattice with N^2 ancilla qubits can, using local qubit operations, simulate a fermionic lattice Hamiltonian [18]. That is, rather than producing long strings of Pauli terms of weight $\mathcal{O}(N)$ that wind around the qubit lattice (as in, for example, Figure 29), the auxiliary qubit mappings produce operations of weight $\mathcal{O}(1)$ and act on adjacent qubits. This comes at the cost of using twice as many qubits as in the original simulation.

In Section IV A, we describe Steudtner and Wehner's template for auxiliary qubit mappings [28]. In Section IV B, we give an example of this process in the form of a new auxiliary qubit mapping. We augment the Mitchison-Durbin pattern to achieve a 37.9% reduction over the S-pattern's average Pauli weight, using only two extra qubits. Thus, taking advantage of the Mitchison-Durbin pattern we see that a constant number of additional qubits almost triples the advantage provided by Theorem 1.

A. Auxiliary qubit mappings

Steudtner and Wehner's formulation of auxiliary qubit mappings¹ [28] is thus: suppose that a fermion-qubit

mapping produces the qubit Hamiltonian

$$H = \sum_{h \in \Gamma} c_h h \,, \tag{64}$$

where $\Gamma \subset \{1, X, Y, Z\}^{\otimes n}$, and $c_h \in \mathbb{C}$ ensure that H is Hermitian, acts on an n-qubit data system (which we denote by the subscript 'dat'). Given a state $|\psi\rangle_{\mathrm{dat}}$ of the qubit system, the goal is to simulate time evolution $e^{-iHt} |\psi\rangle_{\mathrm{dat}}$ using as local a Hamiltonian as possible. An auxiliary qubit mapping achieves this goal using ancilla qubits in an auxiliary register (which we denote by the subscript 'aux'). The following three steps detail how to construct a straightforward type of auxiliary qubit mapping along with the requirements in order for it to function.

1. Choose a subset $\Gamma_{\text{non-loc}} \subset \Gamma$ of terms in the Hamiltonian H. These are the terms which the auxiliary qubit mapping will shorten. For each $h \in \Gamma_{\text{non-loc}}$, choose a Pauli string p^h where $h = h_{\text{loc}} p^h$ such that the weight of h_{loc} is less than that of h. In total, only use r distinct p-strings. That is, several $h \in \Gamma_{\text{non-loc}}$ may contain the same p^h .

Denote the set of all p^h by $\{p_i\}_{i=1}^r$. That is, for any $h \in \Gamma_{\text{non-loc}}$, then $p^h = p_i$ for some $i \in \{1, \dots, r\}$.

2. Introduce r ancilla qubits in the auxiliary register, and devise a unitary mapping

$$V: |\psi\rangle_{\text{dat}} |0\rangle_{\text{aux}}^{\otimes r} \mapsto |\widetilde{\psi}\rangle_{\text{dat,aux}}$$
 (65)

where $|\widetilde{\psi}\rangle_{\mathrm{dat,aux}}$ is such that for each $i\in\{1,\ldots,r\}$, there exists $\sigma_i\in\{\mathbbm{1},X,Y,Z\}$ acting on the ith auxiliary qubit such that

$$((p_i)_{\rm dat} \otimes (\sigma_i)_{\rm aux})|\widetilde{\psi}\rangle_{\rm dat,aux} = |\widetilde{\psi}\rangle_{\rm dat,aux} \ . \tag{66}$$

The $p_i \otimes \sigma_i$ are the *stabilisers* of the combined data and auxiliary system.

Requirement 1: The choice of $\{p_i\}_{i=1}^r$ must allow for the existence of $|\widetilde{\psi}\rangle_{\text{dat,aux}}$ obeying Equation 66. A necessary but insufficient condition is that $[p_i, p_j] = 0$ for all $i, j \in \{1, \dots, r\}$.

3. Modify each $h \in \Gamma$ via

$$h_{\rm dat} \longmapsto h_{\rm dat} \otimes \kappa_{\rm aux}^h$$
, (67)

where κ^h is a Pauli string acting on the auxiliary qubits such that

$$[h_{\rm dat} \otimes (\kappa^h)_{\rm aux}, (p_i)_{\rm dat} \otimes (\sigma_i)_{\rm aux}] = 0$$
 (68)

for all $i \in \{1, ..., r\}$. The rationale for this step is as follows: Suppose that $h = h_{\text{loc}} p^h$, where $p^h = p_i$. Then, we can multiply each $h = h_{\text{loc}} p^h \in \Gamma_{\text{non-loc}}$ by its corresponding stabiliser,

¹ The Verstraete-Cirac mapping uses stabilisers that are of the form $p_{\rm dat} \otimes \tau_{\rm aux}$ where $\tau_{\rm aux}$ acts on more than one qubit [18].

thus producing a lower-weight Hamiltonian term, $((h_{loc})_{dat} \otimes (\sigma_i)_{aux})$:

$$(h_{\text{dat}} \otimes \mathbb{1}_{\text{aux}}) |\widetilde{\psi}\rangle_{\text{dat,aux}}$$

$$= ((h_{\text{loc}} p^h)_{\text{dat}} \otimes \mathbb{1}_{\text{aux}}) |\widetilde{\psi}\rangle_{\text{dat aux}}$$
(69)

$$= \left((h_{\text{loc}} p_i)_{\text{dat}} \otimes \mathbb{1}_{\text{aux}} \right) |\widetilde{\psi}\rangle_{\text{dat aux}} \tag{70}$$

$$= ((h_{\rm loc} p_i)_{\rm dat} \otimes \mathbb{1}_{\rm aux})$$
 (71)

$$((p_i)_{\text{dat}} \otimes (\sigma_i)_{\text{aux}}) |\widetilde{\psi}\rangle_{\text{dat,aux}}$$

$$= ((h_{\text{loc}})_{\text{dat}} \otimes (\sigma_i)_{\text{aux}}) |\widetilde{\psi}\rangle_{\text{dat,aux}}.$$
 (72)

To replicate the time evolution $e^{-iHt} |\psi\rangle_{\rm dat}$ of the system, it is necessary to be able to generate any stabiliser $((p_j)_{\rm dat} \otimes (\sigma_j)_{\rm aux})$ at the step in Equation 71 and commute it past any Hamiltonian term $h_{\rm dat} \otimes \mathbb{1}_{\rm aux}$ where h can now be any element of Γ . If $[h_{\rm dat} \otimes \mathbb{1}_{\rm aux}, (p_j)_{\rm dat} \otimes (\sigma_j)_{\rm aux}] = [h, p_j] \neq 0$, then application of the Hamiltonian term produces a state

$$|\widetilde{\psi}'\rangle_{\mathrm{dat\ aux}} = (h_{\mathrm{dat}} \otimes \mathbb{1}_{\mathrm{aux}}) |\widetilde{\psi}\rangle_{\mathrm{dat.aux}}$$
 (73)

that no longer satisfies Equation 66 for all i, and thus it is impossible to generate and apply more stabilisers as required by Equation 71.

Requirement 2: Crucially, the κ^h must be such that they preserve the time evolution of the data system. That is,

$$V^{\dagger}(h_{\text{dat}} \otimes (\kappa^{h})_{\text{aux}}) |\widetilde{\psi}\rangle_{\text{dat,aux}}$$

$$= h |\psi\rangle_{\text{dat}} \otimes |0\rangle_{\text{aux}}^{\otimes r} .$$
(74)

Otherwise, the system would not retain any useful information. The requirement for the existence of κ^h for $h \in \Gamma$ places a restriction on V.

After satisfying the above three steps, observe that

$$\left(e^{-iHt}\left|\psi\right\rangle_{\rm dat}\right)\otimes\left|0\right\rangle_{\rm aux}^{\otimes r}=\left(V^{\dagger}e^{-i\widetilde{H}t}\right)\left|\widetilde{\psi}\right\rangle_{\rm dat,aux}\;,\eqno(75)$$

where the effective qubit Hamiltonian \widetilde{H} achieves the goal of reducing the Pauli weight of the strings in $\Gamma_{\rm non-loc}$, and acts on both the data and auxiliary systems:

$$\widetilde{H} = \sum_{h \in \Gamma_{\text{non-loc}}} c_h ((h_{\text{loc}})_{\text{dat}} \otimes (\kappa^h \sigma^h)_{\text{aux}})$$

$$+ \sum_{h \in \Gamma \setminus \Gamma_{\text{non-loc}}} c_h (h_{\text{dat}} \otimes (\kappa^h)_{\text{aux}}).$$
(76)

In Equation 76, the Pauli matrix σ^h is the matrix σ_i from the stabiliser $p_i \otimes \sigma_i$ corresponding to $h = h_{\rm loc} \, p^h$ via $p^h = p_i$. Assuming the cost of implementing V is insignificant compared to cost of implementing time evolution by \widetilde{H} , then Equation 75 shows the advantage of the auxiliary qubit mapping: $V^{\dagger}e^{-i\widetilde{H}t}$ is less costly to implement than e^{-iHt} .

B. Using 2 ancilla qubits to reduce average Pauli weight by 37.9% compared to the S-pattern

By modifying the proposal in Theorem 1, it is possible to use the Mitchison-Durbin pattern to produce a 'super-efficient' mapping for square fermionic lattices that is significantly more local, using just $N^2 + 2$ qubits. The result presented here has an average Pauli weight approximately 27.9% less than our result in Theorem 1, and 37.9% less than that of the original S-pattern in [18].

Begin by observing that the edgesum $C^1(f_M)$ of the Mitchison-Durbin pattern has two costly contributions: the $\mathcal{O}(x^2N)$ -valued difference between adjacent vertices in the AD- and DG-interfaces as labelled in Figure 20. We will construct an auxiliary qubit mapping to reduce the contributions of these edges to $C^1(f_M)$.

Take the Hamiltonian of the form Equation 12,

$$H_{\text{fermion}} = \sum_{(\beta,\gamma)\in E} c_{\beta\gamma} a_{\beta}^{\dagger} a_{\gamma} + \text{quartic terms}, \qquad (77)$$

where $G_{\rm F}=(V,E)$ is the $N\times N$ square lattice and $c_{\beta\gamma}\in\mathbb{C}$. Supposing, as in Section II D, that the quartic terms become local Pauli operations, we need only consider the Jordan-Wigner transform of the hopping terms:

$$H = \sum_{(i,j)\in E} c_{ij} h_{ij} =: \sum_{h\in\Gamma} c_h h, \qquad (78)$$

where Γ is the set of Pauli strings produced by using the Mitchison-Durbin pattern to enumerate the fermionic modes in the lattice, as in Figure 8. The previous value for $x \ (\approx 0.29N)$ from Corollary 5.1 only minimises $C^1(f_{\rm M})$ in the ancilla-free case; we must now treat $x \in \{1, 2, \ldots, N/2\}$ once again as a variable, its optimal value currently unknown.

Our fermion-qubit mapping uses a similar approach to the E-type auxiliary qubit mapping from [28]. We will follow the formulation of auxiliary qubit mappings from Section IV:

1. Choose p-strings $\{p_1, p_2\}$ that correspond to the longest individual strings of Pauli-Z matrices of any term $h \in \Gamma$. In this case, we choose

$$p_1 = \left(\bigotimes_{i=x(x-1)+2}^{xN} Z_i\right) \otimes \left(\bigotimes_{\text{other}} \mathbb{1}_i\right) \tag{79}$$

$$p_2 = \left(\bigotimes_{i=(N-x)N+1}^{N^2-x^2+x-1} Z_i\right) \otimes \left(\bigotimes_{\text{other } i} \mathbb{1}_i\right). \tag{80}$$

These bridge the gaps between the outermost vertices on the AD- and DG-interfaces, respectively. Figure 24 depicts the two p-strings for differing values of x; the indices of the first and last qubits of each p-string result from inspecting the label guide in Figure 21.

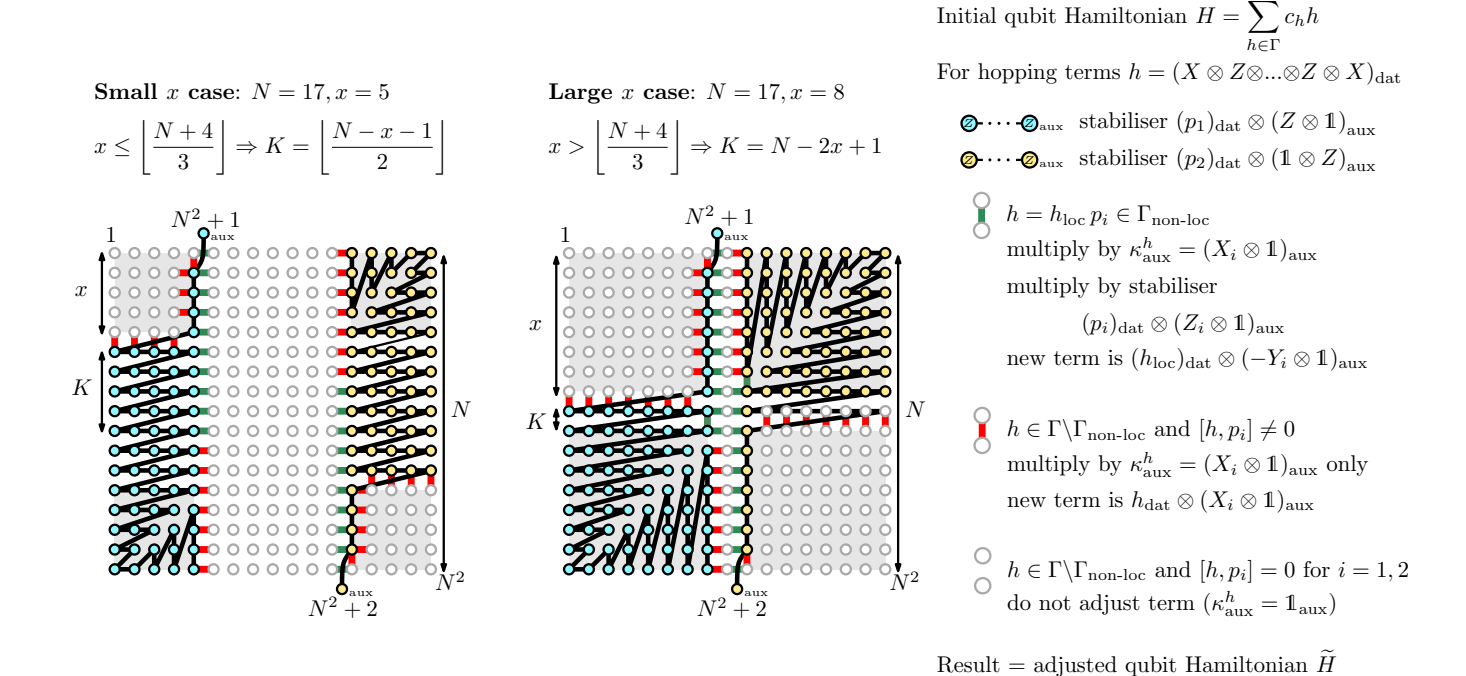


Figure 24: Stabilisers and adjusted Hamiltonian hopping terms for the auxiliary qubit mapping using our augmented Mitchison-Durbin pattern, ' f_{M+2} '. Initialising the (N^2+2) -qubit system in a state stabilised by the strings $p_i \otimes \sigma_i$ nullifies the most costly contributions to the edgesum of the Mitchison-Durbin pattern, resulting in a significantly more local Hamiltonian \widetilde{H} . As the text details, setting $x \approx 0.40N$ results in the lowest average Pauli weight for \widetilde{H} .

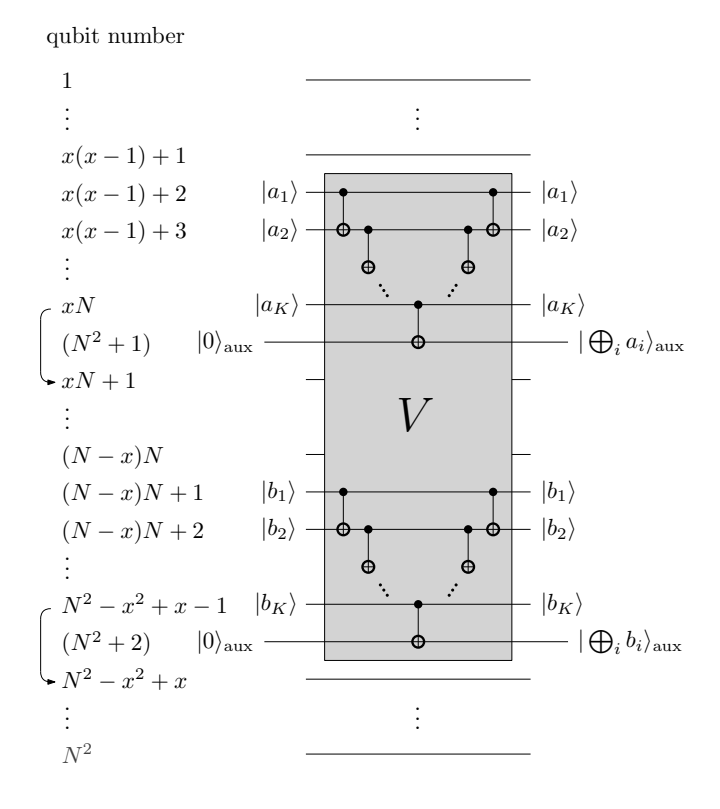


Figure 25: A circuit for V, which initialises the stabiliser state $|\widetilde{\psi}\rangle_{\rm dat,aux}$ from $|\psi\rangle_{\rm dat}|0\rangle_{\rm aux}^{\otimes 2}$ while preserving the time-evolution of the underlying data system.

Then, define $\Gamma_{\text{non-loc}}$ to be all the Hamiltonian terms $h \in \Gamma$ that contain less Z matrices upon multiplication by either p_1 or p_2 . Note that none of the $h \in \Gamma$ would benefit from multiplication by both p-strings, unless x = N/2 exactly as there is no column of vertices separating the stabilisers. Figure 26 shows this in detail with N=6 and x=3. These p-strings trivially satisfy **Requirement 1**'s preliminary condition that $[p_1, p_2] = 0$.

2. Introduce two auxiliary qubits, labelled $N^2 + 1$ and $N^2 + 2$. Define the unitary mapping V to be a cascade of controlled-NOT operations, storing the net parity of the qubits appearing in p_i in the phase of the ith auxiliary qubit. Figure 25 shows a valid circuit for V.

For any input state $|\psi\rangle_{\rm dat}$ of the original N^2 -qubit system, now consider the state

$$|\widetilde{\psi}\rangle_{\mathrm{dat,aux}} = V |\psi\rangle_{\mathrm{dat}} |0\rangle_{\mathrm{aux}}^{\otimes 2} .$$
 (81)

This state has two stabilisers:

$$((p_1)_{\rm dat} \otimes (Z \otimes 1)_{\rm aux}) |\widetilde{\psi}\rangle_{\rm dat,aux} = |\widetilde{\psi}\rangle_{\rm dat,aux} , \quad (82)$$

$$((p_2)_{\rm dat} \otimes (\mathbb{1} \otimes Z)_{\rm aux}) |\widetilde{\psi}\rangle_{\rm dat,aux} = |\widetilde{\psi}\rangle_{\rm dat,aux} . \quad (83)$$

The existence of the stabiliser state $|\widetilde{\psi}\rangle_{\rm dat,aux}$ satisfies **Requirement 1**.

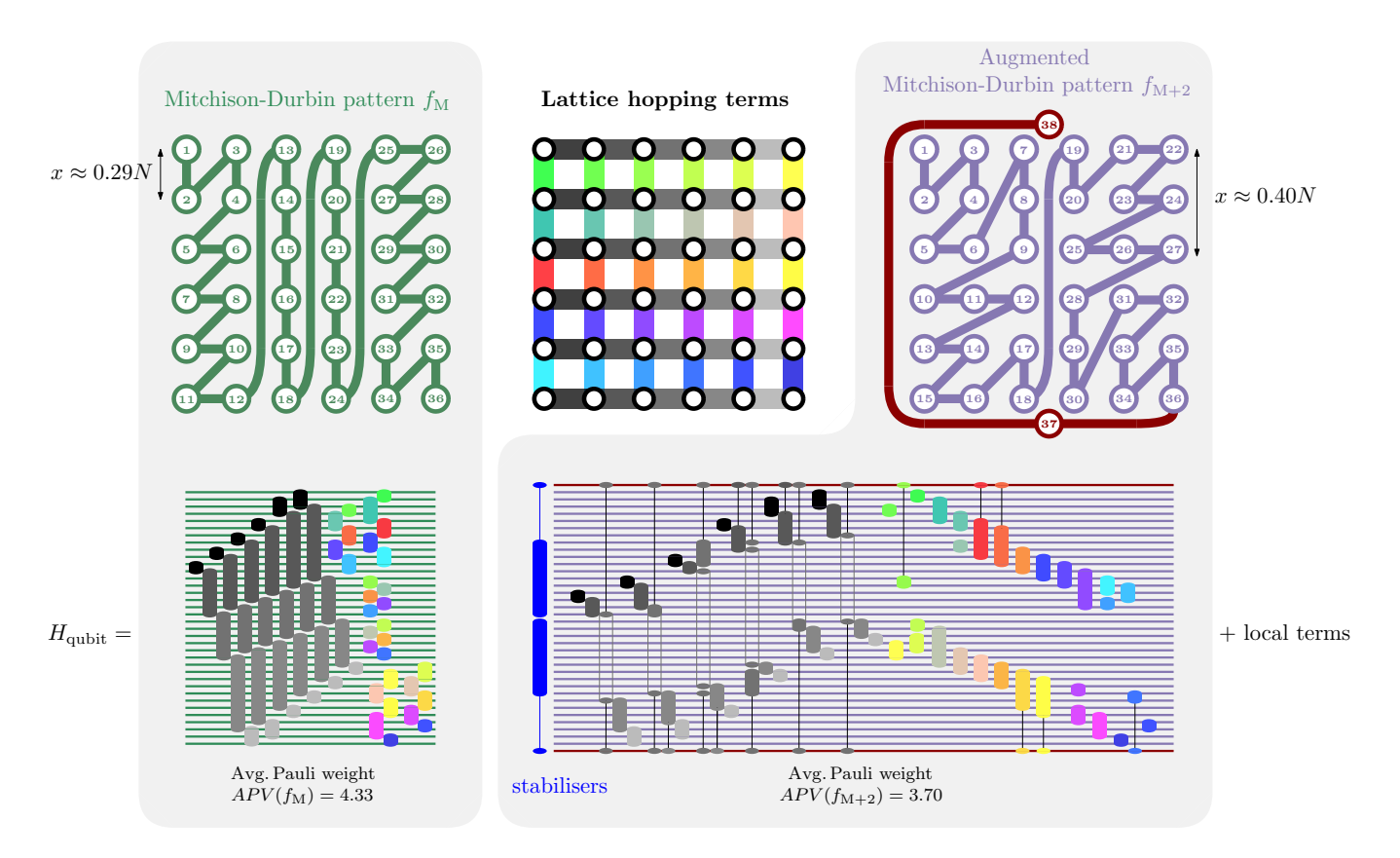


Figure 26: Comparison between the average Pauli weights of Jordan-Wigner mappings generated by the Mitchison-Durbin pattern $f_{\rm M}$ (left) and our auxiliary qubit pattern $f_{\rm M+2}$ (right). The bottom right image shows the reduction of the Pauli weight of long hopping terms after multiplication by stabilisers. Terms that partially overlap the stabilisers must also be adjusted.

3. To identify which terms $h \in \Gamma$ do not commute with p_1 and p_2 , recall from Equation 16 that, without loss of generality, hopping terms have the form

$$h_{\text{dat}} = (X \otimes Z \otimes \cdots \otimes Z \otimes X) \otimes \left(\bigotimes_{\text{other}} \mathbb{1}\right).$$
 (84)

As p_1 and p_2 comprise only Z matrices, $[h, p_i] = 0$ if and only if the Pauli string XZZ...ZX of h intersects completely, or not at all, with the Pauli string ZZZ...Z of p_i , because $[X,Z] = -2Y \neq 0$. Thus the vast majority of the hopping terms already commute with both p-strings; it is only the hopping terms that have one end 'in' p_i and one end 'out of' p_i that need to change. If $[h, p_1] \neq 0$, make the adjustment

$$h_{\rm dat} \longmapsto h_{\rm dat} \otimes (X \otimes \mathbb{1})_{\rm aux} \; ; \tag{85}$$

if $[h, p_2] \neq 0$, make the adjustment

$$h_{\mathrm{dat}} \longmapsto h_{\mathrm{dat}} \otimes (\mathbb{1} \otimes X)_{\mathrm{aux}} .$$
 (86)

If x = N/2 exactly, then some of the horizontal hopping terms across the BD- and DF-interfaces will not commute with either p_1 or p_2 , and need

both adjustments (as depicted in Figure 26). Abbreviating each correction by κ^h , adjusted Hamiltonian terms then satisfy

$$[h_{\text{dat}} \otimes \kappa_{\text{aux}}^h, (p_i)_{\text{dat}} \otimes (\sigma_i)_{\text{aux}}] = 0$$
 (87)

for i = 1, 2 because $[X_{\text{dat}} \otimes X_{\text{aux}}, Z_{\text{dat}} \otimes Z_{\text{aux}}] = 0$. Figure 24 shows which hopping terms need adjustment in this way.

Finally, check that V and κ^h satisfy **Requirement** 2. Let h be a hopping term that does not commute with p_1 . Consider an arbitrary input state

$$|\psi\rangle_{\text{dat}} = \sum_{\vec{a},\vec{b}} \gamma |a_1 a_2 \dots, b_1 b_2 \dots, c_1 c_2 \dots\rangle_{\text{dat}} , \quad (88)$$

where $a_j, b_j, c_j \in \{0, 1\}$ such that \vec{a} contains the parities of all the qubits involved in p_1 , \vec{b} contains the parities of the qubits not involved in either p-string, and \vec{c} contains the parities of the qubits involved in p_2 . The coefficient $\gamma \in \mathbb{C}$ depends on the bit strings \vec{a} , \vec{b} and \vec{c} .

As h does not commute with p_1 , it must contain an X corresponding to one qubit from \vec{a} and one from either \vec{b} (if x < N/2) or \vec{c} (if x = N/2 exactly). Consider the case x < N/2 and let these endpoint

qubits be the jth and kth qubits in each string, respectively. Therefore, the output of $h |\psi\rangle_{\rm dat}$ is

$$h |\psi\rangle_{\text{dat}} = \sum_{\vec{a},\vec{b}} \gamma' |a_1...\overline{a_j}..., b_1...\overline{b_k}..., c_1c_2...\rangle_{\text{dat}}, \quad (89)$$

where γ' is equal to γ up to a sign depending on the effect of the Z matrices in h. Meanwhile, our prescription for κ^h is to apply an X on the first auxiliary qubit. Noting that $V = V^{\dagger}$, observe that

$$V(h \otimes \kappa^h) |\widetilde{\psi}\rangle = V(h \otimes \kappa^h) \sum_{\vec{a}, \vec{b}} \gamma |a_1 a_2 ..., b_1 b_2 ..., c_1 c_2 ...\rangle_{\text{dat}} \otimes (|\oplus_l a_l\rangle |\oplus_l c_l\rangle)_{\text{aux}}$$

$$(90)$$

$$= V \sum_{\vec{a}, \vec{b}} \gamma' \left| a_1 ... \overline{a_j} ..., b_1 ... \overline{b_k} ..., c_1 c_2 ... \right\rangle_{\text{dat}} \otimes \left(\left| \overline{\bigoplus_l a_l} \right\rangle \left| \bigoplus_l c_l \right\rangle \right)_{\text{aux}}$$

$$(91)$$

$$= V \sum_{\vec{a}.\vec{b}} \gamma' \left| a_1 ... \overline{a_j} ..., b_1 ... \overline{b_k} ..., c_1 c_2 ... \right\rangle_{\text{dat}} \otimes \left(\left| a_1 \oplus ... \oplus \overline{a_j} \oplus ... \right\rangle \left| \oplus_l c_l \right\rangle \right)_{\text{aux}}$$
(92)

$$= \sum_{\vec{a},\vec{b}} \gamma' \left| a_1 ... \overline{a_j} ..., b_1 ... \overline{b_k} ..., c_1 c_2 ... \right\rangle_{\text{dat}} \otimes (\left| 0 \right\rangle \left| 0 \right\rangle)_{\text{aux}}$$

$$(93)$$

$$= h \left| \psi \right\rangle_{\text{dat}} \otimes \left| 0 \right\rangle_{\text{aux}}^{\otimes 2} \tag{94}$$

as required. Progressing from Equation 92 to Equation 93 uses fact that V is a cascade of controlled-NOT gates. A symmetric argument follows for all $h \in \Gamma$ which do not commute for p_2 . For the case x = N/2, there will also be Hamiltonian terms that flip a_i and c_k , but a similar argument applies.

This establishes a valid auxiliary qubit mapping. In order to compare the results of this scheme to the ancilla-free approach in Theorem 1, and to the original S-pattern proposal in [18], let us compute the Hamiltonians' average Pauli weight.

The total Pauli weight of all terms in the modified Hamiltonian \widetilde{H} is (1) the cost of the original H, plus (2) the difference between the new and old Z-matrix counts of the terms in $\Gamma_{\text{non-loc}}$ after multiplication by stabilisers, plus (3) the cost of extra operations on the auxiliary qubits from making the κ^h adjustments to terms in $\Gamma \setminus \Gamma_{\text{non-loc}}$. That is,

Total Pauli weight of \widetilde{H} (95)

- = (1) Total Pauli weight of H
 - + (2) difference in Z matrix count of \widetilde{H} and H
 - + (3) number of adjusted terms in \widetilde{H} that are not multiplied by stabilisers

Begin by only considering the effects of the first stabiliser, $(p_1)_{\rm dat} \otimes (Z \otimes \mathbb{1})_{\rm aux}$.

For (1), recall from Equation 24 that the total Pauli weight of the square lattice qubit Hamiltonian H is $C^1(f_{\rm M}) + 2N(N-1)$.

For (2): we explain which hopping terms should be multiplied by stabilisers here. In the original Hamiltonian H, a term $h \in \Gamma$ between vertices α and β of G_F

has Pauli weight $|f_{\rm M}(\alpha) - f_{\rm M}(\beta)| + 1$; as hopping terms consist of a string of Z matrices between a pair of X or Y matrices, the total number of Z matrices in such a term is then

$$\#(Z \text{ matrices in } h) = |f_{\mathcal{M}}(\alpha) - f_{\mathcal{M}}(\beta)| - 1. \tag{96}$$

Referring to the region labels A,B,...,D in Figure 21, it is clear that all of the lengthy hopping terms between vertices on the AD-interface will have less Z matrices after multiplication by the stabiliser $(p_1)_{\rm dat} \otimes (Z \otimes 1)_{\rm aux}$. Using the labels from Figure 21 in Equation 96, the original number of Z matrices in each of these terms is then

#(Z matrices in each hopping term of AD, before)
$$= Nx - x(x-1) - 1.$$
(97)

By inspection, the topmost hopping term across the AD-interface after multiplication by $(p_1)_{\text{dat}} \otimes (Z \otimes 1)_{\text{aux}}$ will consist of a single Z matrix on the first auxiliary qubit. For the hopping terms across the AD-interface in the jth row beneath the top row, there will be 2j Z matrices after multiplication by $(p_1)_{\text{dat}} \otimes (Z \otimes 1)_{\text{aux}}$, including the one on the auxiliary qubit. Thus, the correction term for the AD-interface is

$$\Delta[\#(Z \text{ matrices in } AD)]$$

$$= 1 - (Nx + 1 - (x(x-1) + 1))$$

$$+ \sum_{j=1}^{x-1} \left(2j - (Nx + 1 - (x(x-1) + 1))\right).$$
(98)

Hopping term across the BD-interface and the first row of the CD-interface may benefit from multiplication by $(p_1)_{\text{dat}} \otimes (Z \otimes \mathbb{1})_{\text{aux}}$. Call the collection of these

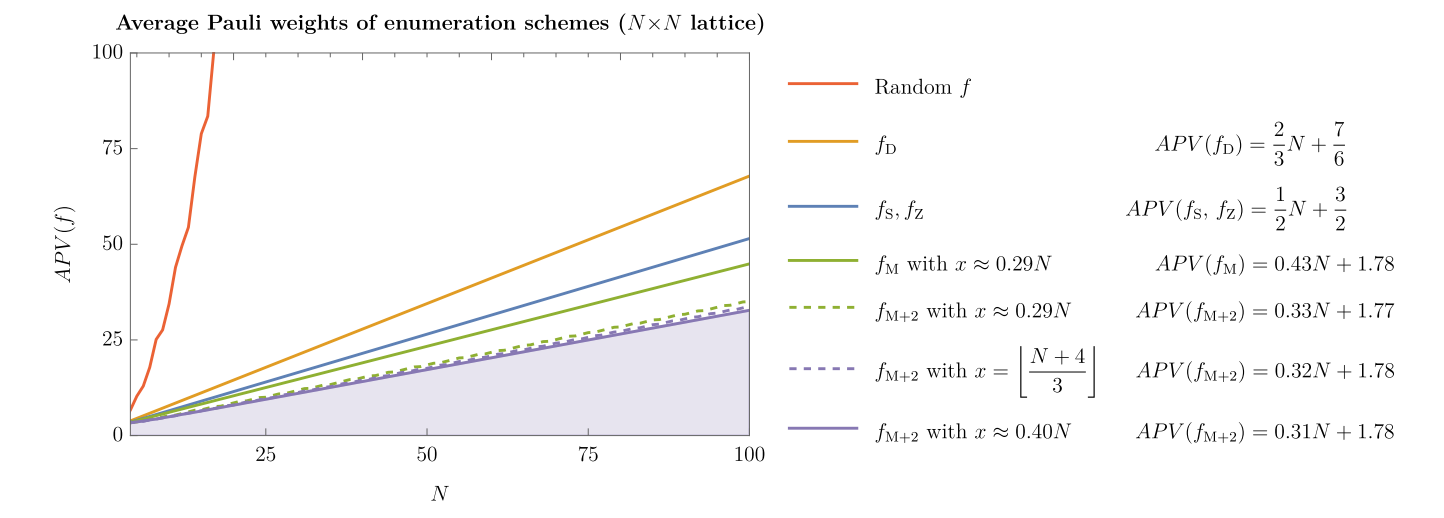


Figure 27: Average Pauli weights APV(f) of enumeration schemes f on $N \times N$ lattices. Random f is a randomly-generated enumeration scheme.

hopping terms the (BC)D-interface, and consider its *i*th row: once again, the labels from Figure 21 in Equation 96 yield

#
$$(Z \text{ matrices in } i \text{th row of } (BC)D, before)$$
 (99)
= $Nx + x + i - (x^2 + ix + 1)$.

By inspection, these terms will have (2+i)x+i-2 Z-matrices after multiplication by the stabiliser $(p_1)_{\rm dat} \otimes (Z \otimes 1)_{\rm aux}$, including the one on the auxiliary qubit.

As Figure 24 shows, if x is large enough then it is possible that a small number of vertical hopping terms within the region C will benefit from stabiliser multiplication as well. Although this reduces the average Pauli weight of the qubit Hamiltonian even further, its effect is negligible compared to the savings across the (BC)D-interface, and we omit it for simplicity. The correction term for the (BC)D-interface is thus

$$\Delta[\#(Z \text{ matrices in } (BC)D)]$$

$$= \sum_{i=1}^{K} \left((2+i)x + i - 2 - \left(Nx + x + i - (x^2 + ix + 1) \right) \right).$$
(100)

The value K depends on the size of x, as Figure 24 illustrates. From a naïve inspection of Equation 100, the ith row of the (BC)D-interface hopping terms will observe a reduction in Z-matrix count after stabiliser multiplication as long as

$$(2+i)x+i-2 < Nx+x+i-(x^2+ix+1)$$
 (101)

$$i < \frac{1}{2x} + \frac{N - x - 1}{2} \tag{102}$$

$$\leq \frac{N-x-1}{2} \,. \tag{103}$$

This might tempt us to set $K = \lfloor (N-x-1)/2 \rfloor$. However, there are N-2x+1 rows in the (BC)D-interface, so the expression in Equation 100 is only valid if

$$K = \min\left\{ \left\lfloor \frac{N-x-1}{2} \right\rfloor, N-2x+1 \right\}. \tag{104}$$

These two values are equal if $x = \lfloor (N+4)/3 \rfloor$. Figure 24 shows the two scenarios where x is above or below this threshold value.

For (3), note that we must adjust all of the hopping terms h that do not commute with p_1 by multiplication by κ^h , which is a single X matrix targeting the first auxiliary qubit. However, in (2) we have already accounted for the cost of an extra auxiliary Z matrix on each of the terms in the AD- and BD-interfaces that benefited from stabiliser multiplication. This Z matrix will become (-Y) upon prior adjustment κ^h (multiplication by X). We therefore need only count hopping terms that partially overlap with p_1 : by inspection of Figure 24, the total number of such terms is

#(X matrices from correction to terms) (105)
=
$$2x - 1 + (N - x - K - 1)$$

= $N + x - K - 1$.

As the Mitchison-Durbin pattern is symmetric, the same rules apply when considering the effects of the second stabiliser, $(p_2)_{\text{dat}} \otimes (\mathbb{1} \otimes Z)_{\text{aux}}$. We can now finally substitute these values into Equation 95 and express the total Pauli weight of \widetilde{H} . Note that the factor of 2 in Equation 106 takes into account both stabilisers:

$$\begin{aligned} & \text{Total Pauli weight of } \widetilde{H} \\ &= C^1(f_{\text{M}}) + 2N(N-1) \\ &+ 2\bigg((1 - (Nx - x(x-1) - 1) \\ &+ \sum_{i=1}^{x-1} (2i - (Nx - x(x-1) - 1)) \\ &+ \sum_{i=1}^{K} \big(((2+i)x + i - 2) \\ &- \big(Nx + x + i - (x^2 + ix + 1) \big) \big) \\ &+ N + x - K - 1 \bigg) \,. \end{aligned}$$

For example, using the original optimal value for x of $\approx 0.29N$ and dividing the total Pauli weight by the number of hopping terms, 2N(N-1), the average Pauli weight of our auxiliary qubit mapping, here nicknamed ' $f_{\rm M+2}$ ', produces a dramatic improvement:

$$APV\left(f_{M+2}\big|_{x\approx0.29N}\right)\approx0.33N+1.77$$
 (107)

However, in the scenario $x \leq \lfloor (N+4)/3 \rfloor$ with $K = \lfloor (N-x-1)/2 \rfloor$, the expression in Equation 106 is actually minimised at the extremum $x = \lfloor (N+4)/3 \rfloor$. The average Pauli weight for large N in this instance is:

$$APV\left(f_{M+2}\Big|_{x=\left\lfloor\frac{N+4}{3}\right\rfloor}\right) \approx \frac{26}{81}N + \frac{289}{162}$$
 (108)
= 0.32N + 1.78. (109)

But there is a better value yet for x: in the other scenario, where $x > \lfloor (N+4)/3 \rfloor$, the value of K is N-2x+1. An approximately optimal value for x to minimise the total Pauli weight in this instance is

$$x = \frac{1}{8} \left(7 + N + \sqrt{\frac{15N^2 - 18N - 53}{3}} \right) \tag{110}$$

$$\approx \frac{1}{8} \left(1 + \sqrt{5} \right) N \tag{111}$$

$$=0.40N$$
, (112)

which is the result of replacing floor brackets with normal parentheses in Equation 106. For large N, this yields an average Pauli weight of

$$APV\left(f_{M+2}\big|_{x\approx0.40N}\right)\approx0.31N+1.68.$$
 (113)

It is for this reason that we define the optimal value of x in our new pattern $f_{\rm M+2}$ to be the rounded value of that in Equation 110, i.e. $x\approx 0.40N$.

Comparing our auxiliary qubit mapping to the S-pattern of [18] and the Mitchison-Durbin pattern of The-

Jordan-Wigner transformation

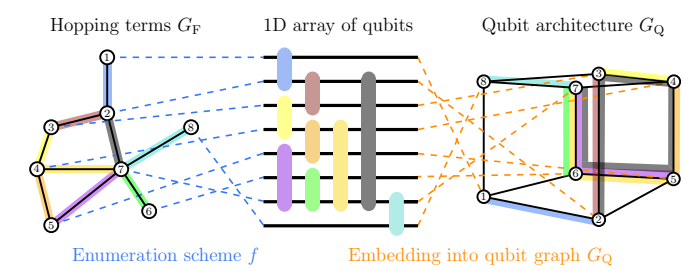


Figure 28: Fermionic enumeration techniques can influence the layout of Pauli strings on nonlinear qubit architectures.

orem 1.

$$\lim_{N \to \infty} \frac{APV(f_{M+2}|_{x \approx 0.40N})}{APV(f_{S})} \approx 0.62$$
 (114)

$$\lim_{N \to \infty} \frac{APV(f_{\rm M+2}|_{x \approx 0.40N})}{APV(f_{\rm M})} \approx 0.72, \qquad (115)$$

yielding a 37.9% improvement over the S-pattern.

Figure 27 shows the average Pauli weights of all the enumeration schemes for the $N\times N$ fermionic lattice discussed in this paper. This analysis does not include the cost of initialising the stabiliser state $|\widetilde{\psi}\rangle_{\text{dat,aux}}$ via the unitary operation V. It is possible to implement V using fewer gates than the circuit in Figure 25 at the cost of more ancilla qubits [51]. However, even adding the cost of the circuit in Figure 25, which is $4(xN-x^2+(x-1))+2$ CNOTs, to Equation 106 has negligible effects on the calculations in this section. The value $x\approx 0.40N$ in Equations 112 still holds.

Figure 26 concludes by demonstrating the advantage of our auxiliary qubit mapping on the 6×6 lattice. When N=6 and x=3, the qubit Hamiltonian \widetilde{H} has a total Pauli weight of 222. (This value slightly different to Equation 106, because the 6×6 lattice has no region D and some hopping terms benefit from multiplication by both stabilisers.) The average Pauli weight is then $\frac{222}{60}=3.70$, which is a 14.6% improvement on the Mitchison-Durbin pattern's ancilla-free optimal average Pauli weight of 4.33 (total Pauli weight 260), and a 17.8% improvement on the S– and Z–patterns' average of 4.5 (total 270).

V. DISCUSSION

A. Summary of results

We have introduced fermionic enumeration schemes as a novel method for improving fermion-qubit mappings, demonstrating two main results.

The first (Section III): when used as enumeration schemes for a Jordan-Wigner transformation, solutions to the edgesum problem can minimise the average Pauli

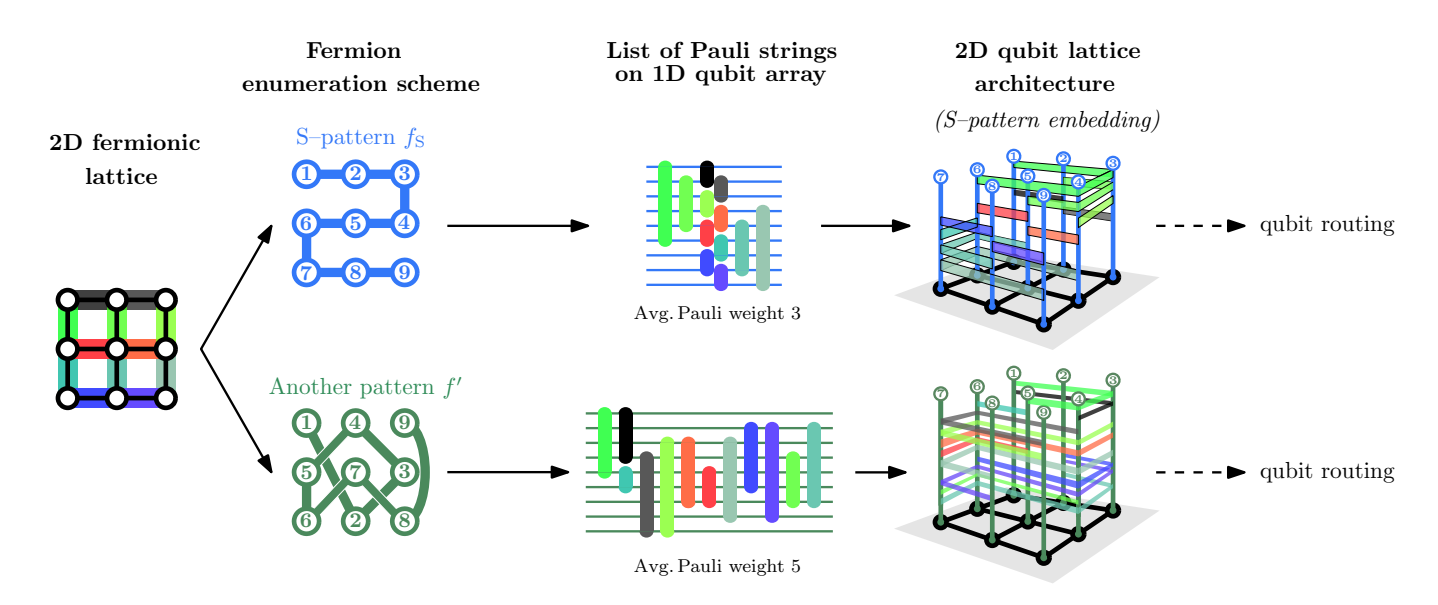


Figure 29: When working with elaborate qubit architectures such as the 2D lattice, the fermionic enumeration scheme need not follow the underlying qubit connectivity. This figure highlights the freedom to choose any scheme to enumerate fermions, yielding averages for the Pauli weights independent of the actual qubit connectivity.

weight of fermionic hopping terms. Theorem 1 illustrates the effect on a 2D fermionic lattice, reducing the average Pauli weight of the hopping terms by 13.9% compared to previous S-pattern methods with the Mitchison-Durbin pattern. Even for fermionic interaction graphs without known edgesum solutions, classical heuristic techniques may provide enumeration schemes that drastically reduce the edgesum, as in the case of cellular arrangements in Section III D.

The second result combines our fermionic enumeration technique with the common strategy of employing auxiliary qubits to further preserve locality of interactions. In Section IV, we provide an improved Mitchison-Durbin pattern for the fermionic square lattice. Uniquely, this mapping requires only two auxiliary qubits, regardless of the number of fermionic modes, and thus effectively improves upon the results of Theorem 1 by reducing the average Pauli weight by 37.9% compared to previous Spattern methods.

Table I compares the ancilla-free Jordan Wigner mappings for the square lattice: Verstraete and Cirac's S-pattern to our optimal ancilla-free mapping using $f_{\rm M}$, and our low-ancilla mapping $f_{\rm M+2}$. Auxiliary qubit mappings with scalable numbers of ancilla qubits are included for comparison. Figure 1 situates the results of Sections III and IV within the existing literature of fermion-qubit mappings.

B. Note on Bravyi-Kitaev and other mappings

The search for more efficient mappings beyond the Jordan-Wigner transformation resulted in the Bravyi-Kitaev transformation [27], which yields exponentially shorter Pauli strings in the asymptotic limit. The Bravyi-Kitaev transformation does not outperform the Jordan-Wigner on modest fermionic systems, however, and has a similar T-gate count [52]. The Jordan-Wigner mapping has gained widespread use because it demands far fewer degrees of connectivity from the qubit architecture [28].

Authors introduced auxiliary qubits to Bravyi-Kitaev mappings [33–35], and, in adiabatic quantum computing protocols, some have also embedded the k–local Hamiltonian problems in higher-dimensional Hilbert spaces through a process called gadgetisation [21]. In the follow-up work, we investigate improvements for the above mappings which emerge when we optimize over fermionic enumeration schemes.

C. Nonlinear qubit architectures and qubit routing

Most of the results that have made use of the Jordan-Wigner and Bravyi-Kitaev transformations rely on qubits with connectivity constraints other than the 1D array. In particular, Verstraete and Cirac [18] pursue a Jordan-Wigner type auxiliary qubit mapping to transform a local Hamiltonian on a fermionic lattice to a local Hamiltonian on a qubit lattice. Subsequent works have followed suit, usually working towards preserving geometric locality between the fermions and qubits, where the assumption is that the qubit architecture is the same as the fermionic graph [28, 34, 35, 50].

Fermionic enumeration schemes influence the distribution of quantum gates throughout nonlinear qubit architectures. To see this, consider decomposing a fermionqubit mapping from a fermionic graph $G_{\rm P}$ to a qubit graph $G_{\rm Q}$ into two components: 1) the *enumeration* of the fermions, which projects the fermionic connectivity graph $G_{\rm F}$ onto a 1D array of qubits, and then 2) the *embedding* of the 1D array of qubits into the qubit architecture $G_{\rm Q}$. Figure 28 visualises the distinction between the two processes.

Verstraete and Cirac's approach is to introduce the S-pattern to enumerate the fermions, and to use an S-pattern embedding to weave Pauli strings into the qubit lattice, as in the top row of Figure 29. In this work we emphasise that these are two distinct processes, and the choice of fermionic enumeration scheme can be done in an entirely separate way to the method of the embedding process. Indeed, as the second row of Figure 29 shows, the path of the fermionic enumeration scheme need not follow the connectivity of the qubit architecture at all to provide a valid mapping.

It is possible to conceive of metrics for fermionic enumeration scheme that do depend on qubit architectures. For example, the qubit routing problem concerns the distribution of Pauli strings on a nonlinear qubit connectivity $G_{\rm Q}$ [53]. In solving this problem for a given could penalise strings of Pauli gates that spread through $G_{\rm Q}$ sparsely, and reward clustered Pauli strings. This poses a different problem to edgesum, as the optimal enumeration scheme for this task will need to take into account the qubit architecture as well. We expect that this is a much more difficult problem to solve than minimising average Pauli weight as we have done here.

Acknowledgements MC is funded by Cambridge Australia Allen and DAMTP Scholarship and the Royal Society PhD studentship. SS acknowledges support from the Royal Society University Research Fellowship scheme.

VI. APPENDIX

A. Edgesum of the S-pattern

Lemma 6. On an $N \times N$ lattice, the S-pattern f_S has edgesum $C^1(f_S) = N^3 - N$.

Proof. Figure 30 displays the S–pattern enumeration procedure for an $N \times N$ grid, as well as the differences between adjacent vertices' indices.

Regardless of whether N is odd or even, the cost is thus

$$C^{1}(f_{S}) = (N-1) \times \text{no. of rows}$$

$$+ \sum_{i=1}^{N} (2i-1) \times (\text{no. of rows} - 1)$$

$$= N^{2} - N + (N-1)(N(N+1) - N)$$

$$= N^{2} - N - N^{2} + N + N(N^{2} - 1)$$

$$= N^{3} - N.$$

$$(116)$$

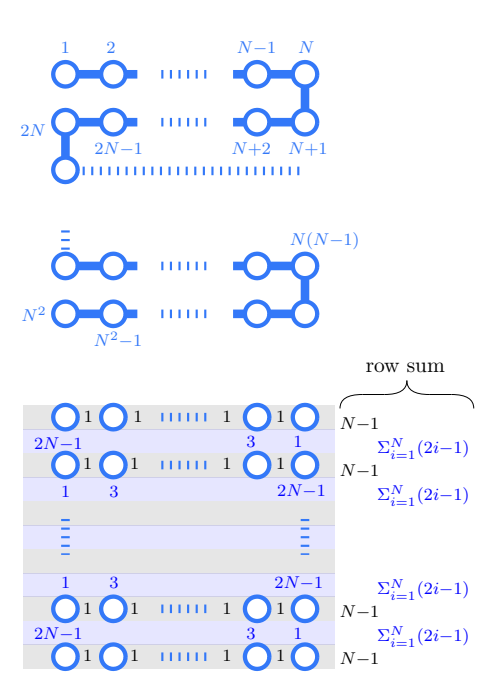


Figure 30: **Top:** S-pattern enumeration on the $N \times N$ square lattice. **Bottom:** Differences between vertex labels using the S-pattern enumeration, with row totals on the far right.

The average Pauli weight for the S-pattern on a square lattice is then

$$APV(f_{\rm S}) = \frac{C^1(f_{\rm S})}{|E|} + 1 = \frac{N^3 - N}{2N(N - 1)} + 1 \qquad (119)$$
$$= \frac{1}{2}N + \frac{3}{2}. \qquad (120)$$

- [1] Graeme Mitchison and Richard Durbin. Optimal numberings of an N×N array. SIAM Journal on Algebraic Discrete Methods, 7(4):571–582, 1986.
- [2] Dave Wecker, Matthew B Hastings, Nathan Wiebe, Bryan K Clark, Chetan Nayak, and Matthias Troyer. Solving strongly correlated electron models on a quantum computer. *Physical Review A*, 92(6):062318, 2015.
- [3] Giacomo Mauro D'Ariano, Franco Manessi, Paolo Perinotti, and Alessandro Tosini. The feynman problem and fermionic entanglement: Fermionic theory versus qubit theory. *International Journal of Modern Physics A*, 29(17):1430025, 2014.
- [4] Nicolai Friis, Antony R Lee, and David Edward Bruschi. Fermionic-mode entanglement in quantum information. Physical Review A, 87(2):022338, 2013.
- [5] Panagiotis Kl Barkoutsos, Nikolaj Moll, Peter WJ Staar, Peter Mueller, Andreas Fuhrer, Stefan Filipp, Matthias Troyer, and Ivano Tavernelli. Fermionic hamiltonians for quantum simulations: a general reduction scheme. arXiv preprint arXiv:1706.03637, 2017.
- [6] Benjamin P Lanyon, James D Whitfield, Geoff G Gillett, Michael E Goggin, Marcelo P Almeida, Ivan Kassal, Jacob D Biamonte, Masoud Mohseni, Ben J Powell, Marco Barbieri, et al. Towards quantum chemistry on a quantum computer. *Nature chemistry*, 2(2):106–111, 2010.
- [7] Manfred Salmhofer. Renormalization in condensed matter: Fermionic systems—from mathematics to materials. Nuclear Physics B, 941:868–899, 2019.
- [8] Christina Verena Kraus. A quantum information perspective of fermionic quantum many-body systems. PhD thesis, Technische Universität München, 2009.
- [9] Ali Hamed Moosavian and Stephen Jordan. Faster quantum algorithm to simulate fermionic quantum field theory. *Physical Review A*, 98(1):012332, 2018.
- [10] Joshua J Goings, Alec White, Joonho Lee, Christofer S Tautermann, Matthias Degroote, Craig Gidney, Toru Shiozaki, Ryan Babbush, and Nicholas C Rubin. Reliably assessing the electronic structure of cytochrome p450 on today's classical computers and tomorrow's quantum computers. arXiv preprint arXiv:2202.01244, 2022.
- [11] Kaoru Hagiwara, K Hikasa, Kenzo Nakamura, M Tanabashi, M Aguilar-Benitez, C Amsler, RMichael Barnett, PR Burchat, CD Carone, C Caso, et al. Review of particle physics. *Physical Review D (Particles and Fields)*, 66(1), 2002.
- [12] Matthew B Hastings and Ryan O'Donnell. Optimizing strongly interacting fermionic hamiltonians. arXiv preprint arXiv:2110.10701, 2021.
- [13] Alán Aspuru-Guzik, Anthony D Dutoi, Peter J Love, and Martin Head-Gordon. Simulated quantum computation of molecular energies. *Science*, 309(5741):1704–1707, 2005.
- [14] Hefeng Wang, Sabre Kais, Alán Aspuru-Guzik, and Mark R Hoffmann. Quantum algorithm for obtaining the energy spectrum of molecular systems. *Physical Chem*istry Chemical Physics, 10(35):5388–5393, 2008.
- [15] Ivan Kassal and Alán Aspuru-Guzik. Quantum algorithm for molecular properties and geometry optimization. The Journal of chemical physics, 131(22):224102, 2009.
- [16] Ivan Kassal, Stephen P Jordan, Peter J Love, Masoud Mohseni, and Alán Aspuru-Guzik. Polynomial-time

- quantum algorithm for the simulation of chemical dynamics. *Proceedings of the National Academy of Sciences*, 105(48):18681–18686, 2008.
- [17] Jarrod R McClean, Ryan Babbush, Peter J Love, and Alán Aspuru-Guzik. Exploiting locality in quantum computation for quantum chemistry. The journal of physical chemistry letters, 5(24):4368–4380, 2014.
- [18] Frank Verstraete and J Ignacio Cirac. Mapping local hamiltonians of fermions to local Hamiltonians of spins. Journal of Statistical Mechanics: Theory and Experiment, 2005(09):P09012, 2005.
- [19] Ivan Kassal, James D Whitfield, Alejandro Perdomo-Ortiz, Man-Hong Yung, and Alán Aspuru-Guzik. Simulating chemistry using quantum computers. Annual review of physical chemistry, 62:185–207, 2011.
- [20] Julia Kempe, Alexei Kitaev, and Oded Regev. The complexity of the local Hamiltonian problem. Siam journal on computing, 35(5):1070–1097, 2006.
- [21] Ryan Babbush, Peter J Love, and Alán Aspuru-Guzik. Adiabatic quantum simulation of quantum chemistry. Scientific reports, 4(1):1–11, 2014.
- [22] Gerardo Ortiz, James E Gubernatis, Emanuel Knill, and Raymond Laflamme. Quantum algorithms for fermionic simulations. *Physical Review A*, 64(2):022319, 2001.
- [23] A Yu Kitaev. Quantum measurements and the abelian stabilizer problem. arXiv preprint quant-ph/9511026, 1995.
- [24] Daniel S Abrams and Seth Lloyd. Quantum algorithm providing exponential speed increase for finding eigenvalues and eigenvectors. *Physical Review Letters*, 83(24):5162, 1999.
- [25] Alberto Peruzzo, Jarrod McClean, Peter Shadbolt, Man-Hong Yung, Xiao-Qi Zhou, Peter J Love, Alán Aspuru-Guzik, and Jeremy L O'brien. A variational eigenvalue solver on a photonic quantum processor. *Nature commu*nications, 5(1):1-7, 2014.
- [26] Jarrod R McClean, Jonathan Romero, Ryan Babbush, and Alán Aspuru-Guzik. The theory of variational hybrid quantum-classical algorithms. New Journal of Physics, 18(2):023023, 2016.
- [27] Sergey B Bravyi and Alexei Y Kitaev. Fermionic quantum computation. Annals of Physics, 298(1):210–226, 2002.
- [28] Mark Steudtner and Stephanie Wehner. Quantum codes for quantum simulation of fermions on a square lattice of qubits. *Physical Review A*, 99(2):022308, 2019.
- [29] Matthew B Hastings, Dave Wecker, Bela Bauer, and Matthias Troyer. Improving quantum algorithms for quantum chemistry. Quantum Information & Computation, 15(1-2):1-21, 2015.
- [30] Pascual Jordan and Eugene Wigner. Über das Paulische Äquivalenzverbot. Zeitschrift fur Physik, 47(9-10):631–651, September 1928.
- [31] Elliott Lieb, Theodore Schultz, and Daniel Mattis. Two soluble models of an antiferromagnetic chain. Annals of Physics, 16(3):407–466, 1961.
- [32] Rami Barends, L Lamata, Julian Kelly, L García-Álvarez, Austin G Fowler, A Megrant, Evan Jeffrey, Ted C White, Daniel Sank, Josh Y Mutus, et al. Digital quantum simulation of fermionic models with a supercon-

- ducting circuit. Nature communications, 6(1):1-7, 2015.
- [33] Kanav Setia, Sergey Bravyi, Antonio Mezzacapo, and James D Whitfield. Superfast encodings for fermionic quantum simulation. Physical Review Research, 1(3):033033, 2019.
- [34] Zhang Jiang, Jarrod McClean, Ryan Babbush, and Hart-mut Neven. Majorana loop stabilizer codes for error mitigation in fermionic quantum simulations. *Physical Review Applied*, 12(6):064041, 2019.
- [35] Charles Derby and Joel Klassen. Low weight fermionic encodings for lattice models. arXiv preprint arXiv:2003.06939, 2020.
- [36] Zhang Jiang, Amir Kalev, Wojciech Mruczkiewicz, and Hartmut Neven. Optimal fermion-to-qubit mapping via ternary trees with applications to reduced quantum states learning. *Quantum*, 4:276, June 2020.
- [37] Michael R Garey, David S Johnson, and Larry Stockmeyer. Some simplified NP-complete problems. In Proceedings of the sixth annual ACM symposium on Theory of computing, pages 47–63, 1974.
- [38] Michael R Garey, Ronald L Graham, David S Johnson, and Donald Ervin Knuth. Complexity results for bandwidth minimization. SIAM Journal on Applied Mathematics, 34(3):477–495, 1978.
- [39] Michael R Garey and David S Johnson. Computers and Intractability; A Guide to the Theory of NP-Completeness. W. H. Freeman & Co., USA, 1990.
- [40] Michael A Nielsen et al. The fermionic canonical commutation relations and the Jordan-Wigner transform. School of Physical Sciences The University of Queensland, 59, 2005.
- [41] Tjalling C Koopmans and Martin Beckmann. Assignment problems and the location of economic activities. *Econometrica: journal of the Econometric Society*, pages 53–76, 1957.
- [42] Steven Bradish Horton. The optimal linear arrangement problem: algorithms and approximation. PhD thesis, School of Industrial and Systems Engineering, Georgia Institute of Technology, 1997.
- [43] Martin Juvan and Bojan Mohar. Optimal linear labelings and eigenvalues of graphs. Discrete Applied Mathematics, 36(2):153–168, 1992.
- [44] Alan George and Alex Pothen. An analysis of spectral envelope reduction via quadratic assignment problems. SIAM Journal on Matrix Analysis and Applications, 18(3):706-732, 1997.
- [45] Yung-Ling Lai and Kenneth Williams. A survey of solved problems and applications on bandwidth, edgesum, and profile of graphs. *Journal of graph theory*, 31(2):75–94, 1999.
- [46] Greg N Frederickson and Susanne E Hambrusch. Planar linear arrangements of outerplanar graphs. *IEEE transactions on Circuits and Systems*, 35(3):323–333, 1988.
- [47] Fan-Rong King Chung. On optimal linear arrangements of trees. Computers & mathematics with applications, 10(1):43-60, 1984.
- [48] James B Saxe. Dynamic-programming algorithms for recognizing small-bandwidth graphs in polynomial time. SIAM Journal on Algebraic Discrete Methods, 1(4):363–369, 1980.
- [49] Nikolaj Moll, Andreas Fuhrer, Peter Staar, and Ivano Tavernelli. Optimizing qubit resources for quantum chemistry simulations in second quantization on a quantum computer. Journal of Physics A: Mathematical and

- Theoretical, 49(29):295301, 2016.
- [50] James D Whitfield, Vojt ĕch Havlíček, and Matthias Troyer. Local spin operators for fermion simulations. Phys. Rev. A, 94:030301, Sep 2016.
- [51] Jiaqing Jiang, Xiaoming Sun, Shang-Hua Teng, Bujiao Wu, Kewen Wu, and Jialin Zhang. Optimal space-depth trade-off of CNOT circuits in quantum logic synthesis. In Proceedings of the Fourteenth Annual ACM-SIAM Symposium on Discrete Algorithms, pages 213–229. SIAM, 2020.
- [52] Andrew Tranter, Peter J Love, Florian Mintert, and Peter V Coveney. A comparison of the bravyi–kitaev and jordan–wigner transformations for the quantum simulation of quantum chemistry. *Journal of chemical theory and computation*, 14(11):5617–5630, 2018.
- [53] Alexander Cowtan, Silas Dilkes, Ross Duncan, Alexandre Krajenbrink, Will Simmons, and Seyon Sivarajah. On the Qubit Routing Problem. In Wim van Dam and Laura Mancinska, editors, 14th Conference on the Theory of Quantum Computation, Communication and Cryptography (TQC 2019), volume 135 of Leibniz International Proceedings in Informatics (LIPIcs), pages 5:1–5:32, Dagstuhl, Germany, 2019. Schloss Dagstuhl-Leibniz-Zentrum fuer Informatik.